nature chemistry

Article

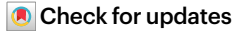
https://doi.org/10.1038/s41557-023-01288-w

Hybrid organic-inorganic two-dimensional metal carbide MXenes with amido- and imido-terminated surfaces

Received: 16 September 2022

Accepted: 29 June 2023

Published online: 3 August 2023



Chenkun Zhou $oldsymbol{0}^{1,2}$, Di Wang $oldsymbol{0}^{1}$, Francisco Lagunas $oldsymbol{0}^{3}$, Benjamin Atterberry 4,5 , Ming Lei $oldsymbol{0}^{6}$, Huicheng Hu 1 , Zirui Zhou $oldsymbol{0}^{1}$, Alexander S. Filatov $oldsymbol{0}^{1}$, De-en Jiang $oldsymbol{0}^{6}$, Aaron J. Rossini $oldsymbol{0}^{4,5}$, Robert F. Klie $oldsymbol{0}^{3}$ & Dmitri V. Talapin $oldsymbol{0}^{1,2,7,8}$

Two-dimensional (2D) transition-metal carbides and nitrides (MXenes) combine the electronic and mechanical properties of 2D inorganic crystals with chemically modifiable surfaces, which provides an ideal platform for both fundamental and applied studies of interfaces. Good progress has been achieved in the functionalization of MXenes with small inorganic ligands, but relatively little work has been reported on the covalent bonding of various organic groups to MXene surfaces. Here we synthesize a family of hybrid MXenes (h-MXenes) that incorporate amido- and imido-bonding between organic and inorganic parts by reacting halogen-terminated MXenes with deprotonated organic amines. The resulting hybrid structures unite tailorability of organic molecules with electronic connectivity and other properties of inorganic 2D materials. Describing the structure of h-MXene necessitates the integration of concepts from coordination chemistry, self-assembled monolayers and surface science. The optical properties of h-MXenes reveal coherent coupling between the organic and inorganic constituents. h-MXenes also exhibit superior stability against hydrolysis.

MXenes^{1,2} are typically synthesized by etching crystalline compounds defined as MAX phases, where M represents an early transition metal (Ti, Nb, V, Mo, etc.), A represents a main group element usually from groups 13–16 (Al, Si, etc.), and X stands for carbon or nitrogen³. MAX phases, for example, Ti₃AlC₂, are converted to two-dimensional (2D) MXenes by selectively etching away A-layer elements, typically using fluoride solutions^{3–5}. The resulting exfoliated MXenes, which show impressive performance as supercapacitors, batteries and electromagnetic interference shielding materials^{1,2}, have a mixture of –F, –O

and -OH surface termination groups, usually denoted as T_x . Unlike surfaces of graphene and transition-metal dichalcogenides, the basal surfaces of MXenes allow for further chemical modification with different functional groups. However, postsynthetic substitutions of surface groups are impeded by the very strong Ti–F and Ti–O bonds introduced during MAX exfoliation with fluoride reagents. An alternative synthetic route, which omits fluoride by transferring the MAX etching process to a molten-salt medium, can produce MXenes with pure -Cl or -Br terminations $^{6-9}$. Ti–Cl and Ti–Br surface bonds are labile enough to allow

¹Department of Chemistry, University of Chicago, Chicago, IL, USA. ²James Franck Institute, University of Chicago, Chicago, IL, USA. ³Department of Physics, University of Illinois Chicago, Chicago, IL, USA. ⁴US Department of Energy, Ames National Laboratory, Ames, IA, USA. ⁵Department of Chemistry, Iowa State University, Ames, IA, USA. ⁶Department of Chemical and Biomolecular Engineering, Vanderbilt University, Nashville, TN, USA. ⁷Pritzker School of Molecular Engineering, University of Chicago, Chicago, IL, USA. ⁸Center for Nanoscale Materials, Argonne National Laboratory, Argonne, IL, USA. ©e-mail: dvtalapin@uchicago.edu

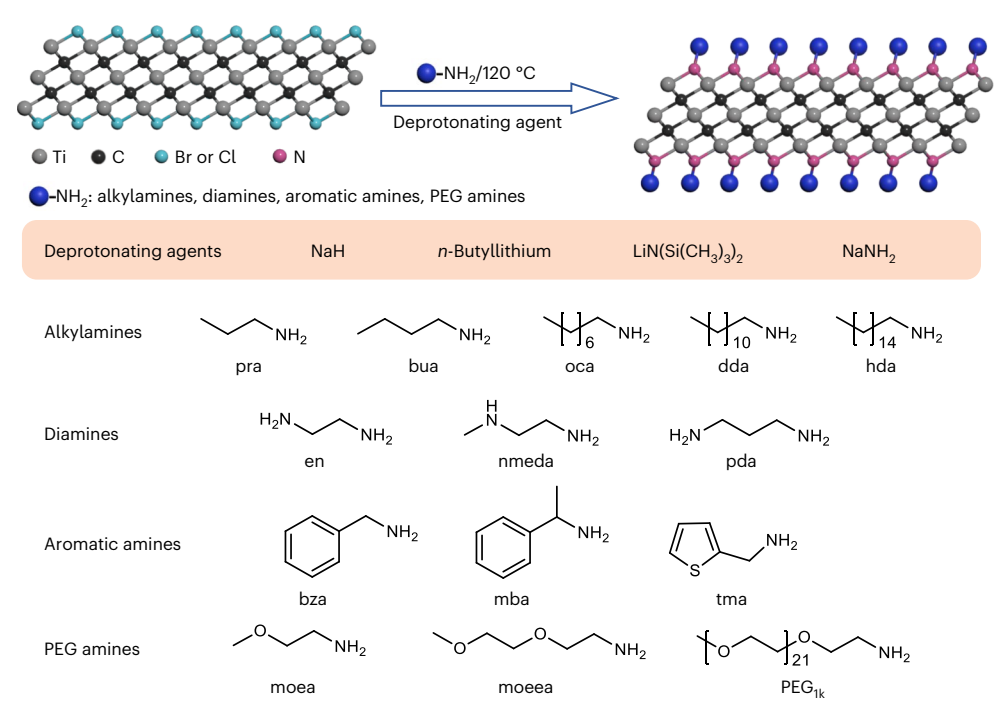


Fig. 1|h-MXene synthesis. Schematic of organic-inorganic h-MXene synthesis and examples of the studied deprotonating agents and organic amines.

the exchange of surface halogen atoms with other groups, and MXenes with pure chalcogenido or imido terminations, and bare MXenes, can all be prepared from $Ti_3C_2Cl_2$ or $Ti_3C_2Br_2$. The surface groups can define MXene properties, such as superconductivity⁶ and electrochemical energy storage capacitance10, and many other physical and chemical properties of MXenes as predicted by theoretical studies¹¹⁻¹³. Here we introduce a general approach toward hybrid organic-inorganic MXenes (h-MXenes) with a broad scope of organic terminal groups.

Results and discussion

Synthesis

h-MXenes can be synthesized via the displacement of halides from Br- or Cl-terminated MXenes by deprotonated primary organic amines (for example, n-alkylamines). The amines are first deprotonated by NaH, *n*-butyllithium, lithium bis(trimethylsilyl)amide or sodium amide, and then reacted with multilayer Ti₃C₂Br₂ MXenes at 120 °C for 2 days (Methods and Supplementary Figs. 1 and 2). The overall reaction between Ti₃C₂Br₂ and amine in the presence of the deprotonating agent NaH is as follows:

$$RNH_2 + NaH + Ti_3C_2Br_2 \rightarrow Ti_3C_2(NR)_r(NHR)_v + H_2(g) \uparrow + NaBr$$

The scope of studied amines is shown in Fig. 1. Complete removal of Br was confirmed by X-ray fluorescence (XRF) analysis (Extended Data Fig. 1a). Deprotonation of amines is crucial to initiate the exchange reaction on MXene surfaces; tertiary amines (for example, triethylamine) showed no reactivity toward halide-terminated MXenes (Extended Data Fig. 1b,c). Identical products were obtained by reacting Ti₃C₂Br₂ and Ti₃C₂Cl₂ with deprotonated butylamine (Extended Data Fig. 2a). Very strong binding of amines to Ti₃C₂ sheets follows from thermogravimetric analysis, which shows that, for example, the n-propylamine-functionalized $Ti_3C_2(pra)_{2/3}$ shows only 4% weight loss when heated from 50 °C to 400 °C (Extended Data Fig. 1d). The structural integrity of inorganic h-MXene sheets was retained up to at least 500 °C, while gradual carbonization of hydrocarbon chains occurred above 400 °C (Extended Data Fig. 1e and Supplementary Figs. 3-5). Besides various alkylamines, this approach has been applied to diamines, aromatic amines and poly(ethylene glycol) (PEG)-amines. Examples of the corresponding h-MXenes are shown in Extended Data Fig. 2b,c. The above reaction can also be applied to Ti₂CCl₂ and Nb₂CCl₂ to obtain organic-inorganic hybrid Ti₂C or Nb₂C MXenes, as shown in Extended Data Fig. 2d.

Investigation of interfacial bonding motifs

To investigate bonding details between the organic and inorganic components of h-MXenes, we employed magic angle spinning (MAS) solid-state NMR spectroscopy (ssNMR), which has proven to be a powerful tool for probing chemical bonding at MXene surfaces (Fig. 2, Supplementary Discussion 1 and Supplementary Figs. 6–11)^{10,14–16}. The one-dimensional ¹H spin echo spectra of ¹⁵N-labelled Ti₃C₂(¹⁵N-dda)_{2/3} h-MXene shows an intense peak at 1 ppm associated with overlapping CH₂ signals from dodecyl alkane hydrogens. In addition, broader and lower-intensity ¹H NMR signals centred at chemical shifts of 9 ppm and 20 ppm are visible (Fig. 2a). The latter is assigned to the NH hydrogen atoms of amido ligands, while the former is tentatively assigned to surface hydride based on a hypothesized pathway of amido to imido conversion (Supplementary Discussion 1 and Supplementary Fig. 10).

The ¹H → ¹5N cross-polarized MAS (CPMAS) spin echo spectrum shows two broad ¹⁵N NMR signals with chemical shifts of 30 ppm and -28 ppm, which are assigned to imido (NR) and amido (NHR) ligands that coordinate to surface titanium atoms, respectively. These assignments are consistent with previously reported ¹⁵N chemical shifts for molecular transition-metal imido and amido complexes, where the former is more positively shifted¹⁷. Peak fitting of the ¹⁵N CPMAS spin echo NMR spectrum suggests that ~58% of the nitrogen atoms are in the imido form, while \sim 42% are in the amido form (Supplementary Fig. 6). The ¹⁵N signal assignments were further confirmed with ¹H{¹⁵N} indirectly detected heteronuclear correlation (idHETCOR) experiments obtained with backwards CP contact times of 0.4 ms or 8 ms to probe shortand long-range ¹H-¹⁵N internuclear distances, respectively (Fig. 2b). As expected, the HETCOR spectrum obtained with a 0.4 ms contact time only shows the amido 15N NMR signal centred at -28 ppm and reveals that it correlates to the ¹H NMR signal at +20 ppm. The HETCOR spectrum obtained with 8 ms contact time shows both imido and amido

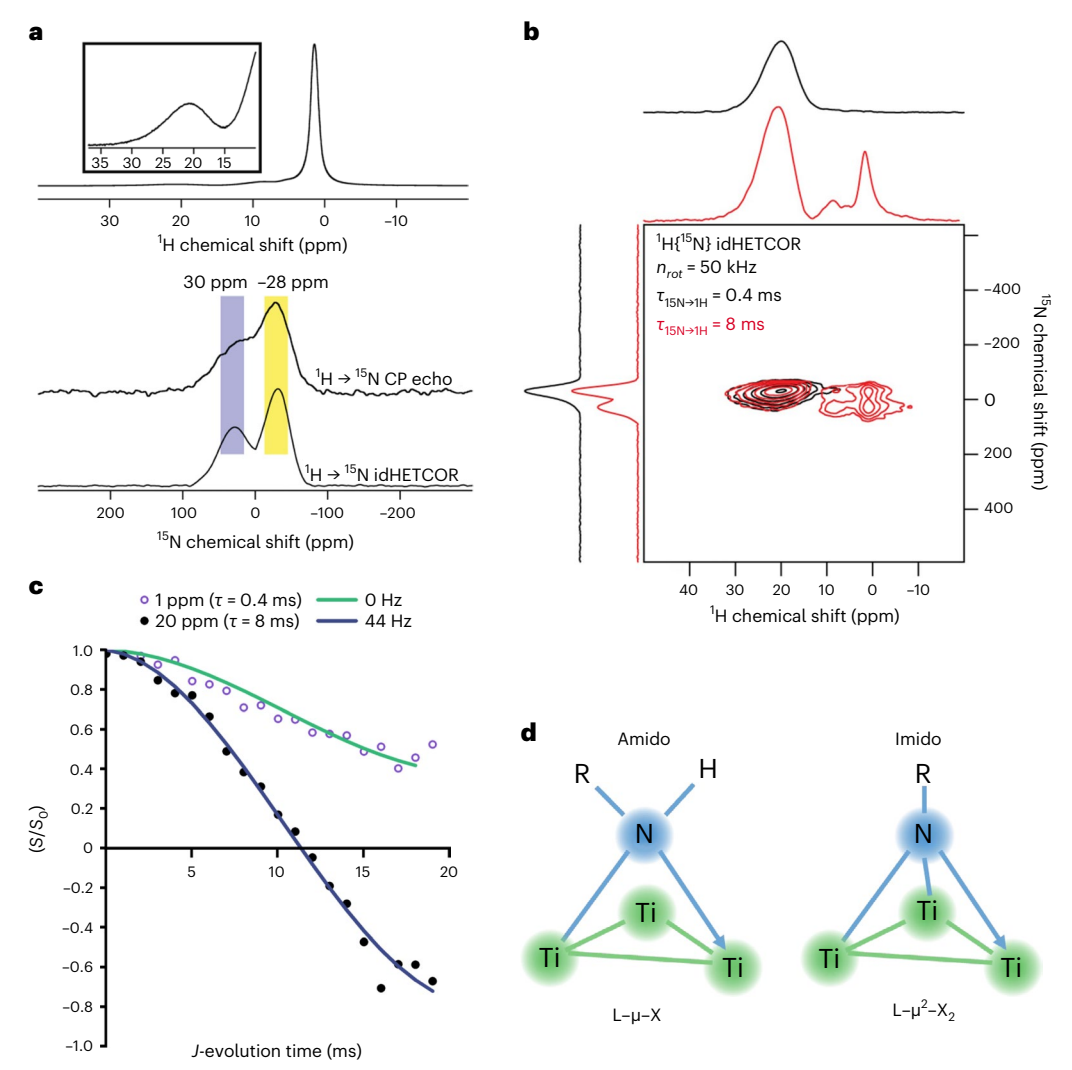


Fig. 2 | Investigation of inorganic – organic bonding in h-MXenes. a, ${}^{1}H$ spin echo, ${}^{1}H \rightarrow {}^{15}N$ CPMAS spin echo and ${}^{1}H$ -detected ${}^{15}N$ CPMAS spectrum of $Ti_{3}C_{2}({}^{15}N-dda)_{2/3}$. b, $2D\,{}^{1}H\{{}^{15}N\}$ idHETCOR spectra obtained with backwards CP contact times of $0.4\,$ ms or $8\,$ ms to probe short- and long-range ${}^{1}H-{}^{15}N$ internuclear distances, respectively. c, ${}^{1}H$ detected ${}^{15}N\{{}^{1}H\}$ heteronuclear spin echo (J-

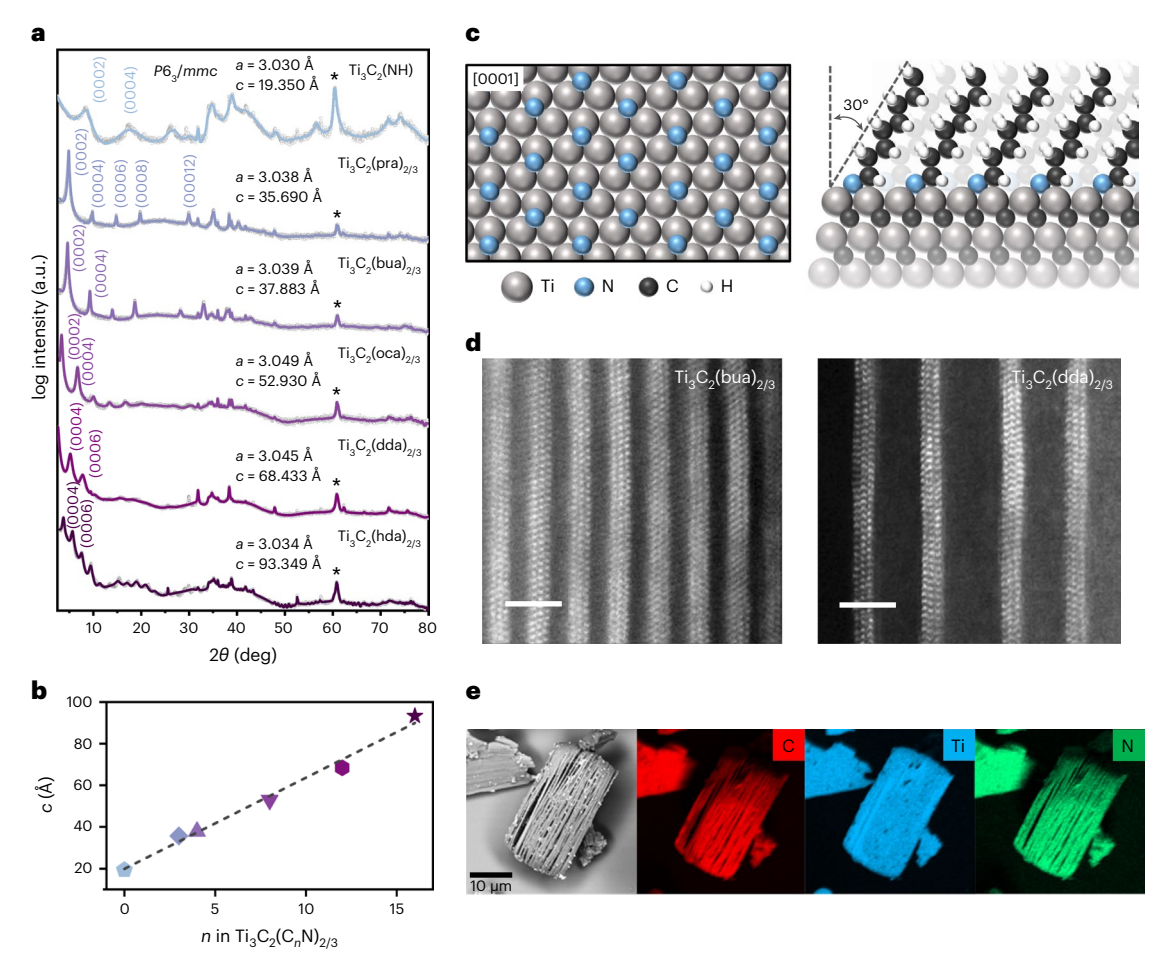
resolved) curves confirming that the 15 N NMR signal at -28 ppm corresponds to an amido nitrogen (NHR), while the 15 N NMR signal at 30 ppm corresponds to a deprotonated imido nitrogen (NR). All spectra were obtained with an MAS frequency of 50 kHz. \mathbf{d} , The bonding motifs between the organic and inorganic components of h-MXenes.

¹⁵N NMR signals. Acquisition of 1D ¹H{¹⁵N} idHETCOR spectra with variable backwards CP contact time allows measurement of ¹H-¹⁵N dipolar coupling constants and estimation of ¹H-¹⁵N internuclear distances (Supplementary Fig. 7)¹⁸. This experiment confirms that the amido hydrogen atom (δ = 20 ppm) has a 1.04 Å N-H internuclear distance and suggests that ¹H hydrogen atoms (δ = 9 ppm) are ~1.9 Å from the amido and imido nitrogen atoms. Finally, ¹H-detected ¹⁵N{¹H} heteronuclear J-resolved spin echo experiments were used to confirm that the amido nitrogen makes a covalent bond to a single hydrogen atom (Fig. 2c). The J-resolved curve obtained by monitoring the amido ¹H NMR signal can be fitted with a cosine function, confirming there is only a single attached hydrogen atom. The fit yields a nitrogen-hydrogen scalar coupling constant (${}^{1}\!J_{NH}$) of 44 Hz. A *J*-resolved curve for alkyl ${}^{1}\!H$ NMR signal obtained with a back-CP contact time of 8 ms can be fitted with two ${}^{1}J_{NH}$ values of 44 Hz and 0 Hz. The latter must correspond to imido nitrogen atoms, as these nitrogen atoms do not have a covalent bond to hydrogen.

MAS-ssNMR studies show the presence of both amido and imido ligands bonded to ${\rm Ti_3C_2}$ sheets. To evaluate the thermodynamic stability of amido and imido motifs, density functional theory (DFT) modelling was used to compute the bond-dissociation energies

(BDEs), defined as the energy change when A-B is cleaved to be A and B fragments (Supplementary Discussion 2). The BDEs for amido $(C_3H_7NH_-)$ and imido $(C_3H_7N_-)$ groups from the $Ti_3C_2(pra)_{2/3}$ (0001) surface have been calculated to evaluate the thermodynamic stability of h-MXenes. For amido (-NHR) surface terminations, although the nitrogen atom is already bonded to one hydrogen atom, the nitrogen atom still tends to interact with three titanium atoms on the (0001) surface after structural relaxation (Extended Data Fig. 3a). The calculated N-H internuclear distance in the amido group is 1.03 Å, which is in a good agreement with the experimental value of 1.04 Å obtained from idHETCOR spectra. For the imido (=NR) case, the nitrogen atom formed three equivalent bonds to titanium atoms. The calculated BDEs of amido and imido ligands are 2.65 eV and 4.73 eV, respectively. The latter BDE is substantially larger than the 3.73 eV required to dissociate one chlorine atom away from the surface of Ti₃C₂Cl₂ MXene, and the formation of strongly bonded imido ligands is probably responsible for the improved stability of h-MXenes discussed below.

The formation of h-MXenes probably starts with a nucleophilic substitution of surface halide terminations for RNH⁻, promoted by the formation of solid sodium halides or lithium halides. Because alkylamines cannot be doubly deprotonated under our experimental



 $\label{eq:fig.3} \textbf{Fig. 3} | \textbf{Structural characterizations of h-MXenes. a}, \textbf{Powder X-ray diffraction} \\ \textbf{patterns and their Le Bail fits for } \textbf{Ti}_3\textbf{C}_2(\textbf{NH}) \text{ and h-MXenes with alkylimido surface-termination groups. (*) shows the } (11\bar{2}\,0) \text{ diffraction peak. b}, \textbf{Changes of the lattice } c \text{ parameter versus number of carbon atoms in the interlayer alkyl groups } (\text{pentagon, } \textbf{Ti}_3\textbf{C}_2(\textbf{NH}); \text{ rhombus, } \textbf{Ti}_3\textbf{C}_2(\text{pra})_{2/3}; \text{ triangle, } \textbf{Ti}_3\textbf{C}_2(\text{bua})_{2/3}; \text{ inverted} \\ \end{aligned}$

triangle, $Ti_3C_2(oca)_{2/3}$; hexagon, $Ti_3C_2(dda)_{2/3}$; star, $Ti_3C_2(hda)_{2/3}$. ${\bf c}$, Schematic of alkylimido surface termination groups on a Ti_3C_2 sheet. ${\bf d}$, Low-angle annular dark-field STEM images showing the lamellar structures of h-MXenes; the image of $Ti_3C_2(dda)_{2/3}$ was acquired using a cryo-STEM method. Scale bar, 2 nm. ${\bf e}$, SEM-EDS element mapping of $Ti_3C_2(bua)_{2/3}$ MXene.

conditions, the conversion from amido to imido bonding is expected to occur at the MXene surface. This process can be described as N–H oxidative addition leading to the formation of imido group and hydride (Supplementary Discussion 1 and Supplementary Fig. 10). Such transformations have precedents in the molecular organometallic zirconium and hafnium compounds 19 . In another valuable insight from organometallic chemistry, the amido groups can be classified as $L-\mu-X$ -type ligands and the imido groups as $L-\mu^2-X_2$ -type ligands using Green's classification of covalent bonds (Fig. 2d and Supplementary Discussion 3) 20 . This classification has been widely used for nanocrystal surfaces, and has proved particularly useful in describing ligand substitution reactions 21 .

Packing geometry of alkyl chains in h-MXenes

Powder X-ray diffraction patterns from Ti_3C_2 -derived h-MXenes with different n-alkyl groups are shown in Fig. 3a. For the purpose of refinement, Ti_3C_2 -derived MXenes can be nominally assigned to the $P6_3/mmc$ space group 22 . Because the probability of elastic X-ray scattering is dominated by heavy atoms, titanium in our case, this structure assignment is useful for La Bail refinement, even if it does not capture the full symmetry of organic surface groups. For comparison, the Ti_3C_2 (pra) $^{2/3}$ powder X-ray diffraction pattern is also fitted using the $P2_1/m$ space group to account for the contribution from the organic surface groups (Supplementary Fig. 13).

The first member of the homologous series of $\text{Ti}_3\text{C}_2(\text{NR})_x(\text{NHR})_y$ MXenes, $\text{Ti}_3\text{C}_2(\text{NH})_x$, where $x \approx 1$, can be synthesized by reacting $\text{Ti}_3\text{C}_2\text{Br}_2$ with NaNH₂. With an increase in the length of alkyl chain, all (0 0 0 l) diffraction peaks of h-MXenes shift to smaller 2θ angles, indicating the expansion of the spacing between Ti_3C_2 layers. Some diffraction peaks, for example, the (0 0 0 10) reflection of $\text{Ti}_3\text{C}_2(\text{pra})_{2/3}$, disappear due to symmetry-related cancellation (Extended Data Fig. 4). The lattice parameters of h-MXenes, calculated using the Le Bail method, show that the lattice constant c linearly increases with the length of alkyl chain (Fig. 3b).

The lattice constant a, which defines the distance between neighbouring titanium atoms on the surface of ${\rm Ti_3C_2}$ sheets, is sensitive to in-plane strain imposed by surface groups and varies with the type and concentration of surface groups 6 . In the ${\rm Ti_3C_2(NR)_x(NHR)_y}$ homologous series, the lattice constant a is practically independent of the alkyl chain length, suggesting that the grafting density of surface ligands is independent of the alkyl group. By coincidence, the interatomic metalmetal distances at the surface of h- ${\rm Ti_3C_2MXenes}(3.04~{\rm Å})$ are very close to those at the Au (111) surface (2.88 Å), and the packing of alkyl chains on these basal planes could resemble the structure of self-assembled monolayers (SAMs) of n-alkanethiol molecules on Au (111) surfaces 23,24 . For the Au (111) surface, the SAM grafting density is limited by the steric bulk of alkyl tails: the organic layer fills the space completely with alkyl tails tilted approximately 30° from the surface normal to maximize their van der Waals interactions (Fig. 3c), whereas surface-bound head

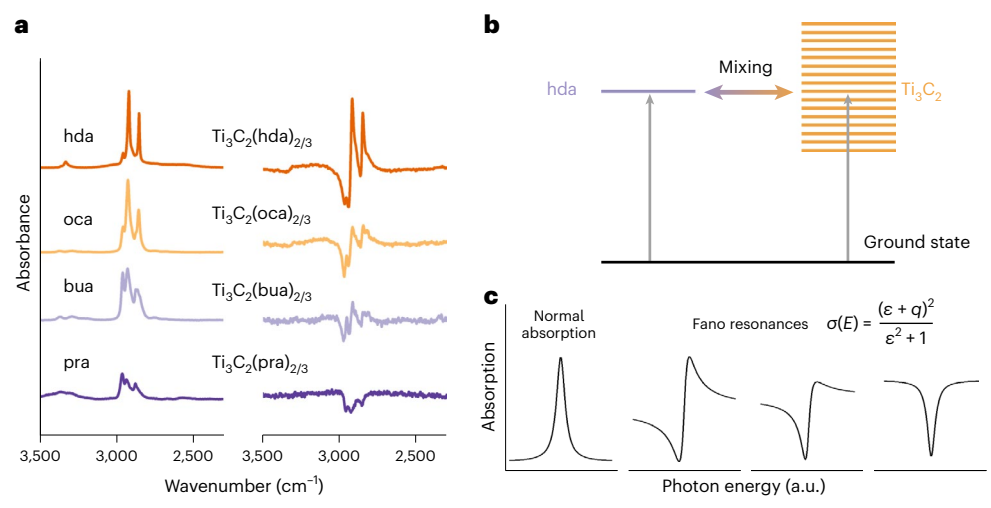


Fig. 4 | **Fano effect in the infrared absorption spectra of h-MXenes. a**, C–H bond stretching region of infrared absorption spectra of h-MXenes with alkylimido surface-termination groups showing the Fano resonant coupling compared to the absorption of neat alkylamines. **b**, Schematic of the Fano coupling between discrete vibrational modes of *n*-alkylamines and the

continuum band of states in metallic Ti_3C_2 sheets. \mathbf{c} , Schematic of absorption spectrum with Lorentzian line shape and Fano resonance showing asymmetric line shape. ε , reduced energy; q, Fano parameter defining the absorption line shape 28,40 .

groups occupy three-fold sites of a $\left(\sqrt{3}\times\sqrt{3}\right)$ $R30^\circ$ lattice²⁴. Such packing would produce a Ti₃C₂(NR)_{2/3} or Ti₃C₂(NHR)_{2/3} stoichiometry for pure imido or amido groups, respectively, independent of alkyl chain length, which is in good agreement with the stoichiometry obtained from the elemental analysis of various h-MXenes, X-ray photoelectron spectroscopy (XPS) survey spectra and computational modelling (Extended Data Fig. 5a, Supplementary Discussions 2 and 4, Supplementary Figs. 12 and 14–18, and Supplementary Tables 1–4).

The spacing between ${\rm Ti_3C_2}$ sheets can be compared to the length of fully extended alkyl chains. The lattice constant c linearly depends on the number of carbon atoms (Fig. 3b), with the slope showing that neighbouring ${\rm Ti_3C_2}$ sheets sandwich two layers of alkyl chains with ~1.10 Å per methylene unit (Extended Data Fig. 5b,c). Since the theoretical length of fully extended alkyl chains with all-trans conformations is ~1.27 Å per CH₂ group²³, the tilt of the alkyl chains in h-MXenes should be close to arccos (1.10 Å/1.27 Å) = 30° from the surface normal, again consistent with the similar packing geometries of alkyl chains in h-MXenes and Au (111) alkanethiol SAMs. The DFT-modelled structurally relaxed surfaces of ${\rm Ti_3C_2}({\rm pra})_{2/3}$ and ${\rm Ti_3C_2}({\rm oca})_{2/3}$ h-MXenes showed the alkyl chains tilted by 34° and 35° from the surface normal, respectively (Extended Data Fig. 3b). The tilt angle of alkyl chains was not affected by the nature of the surface-bound amido or imido group (Supplementary Discussion 2).

Scanning electron microscopy (SEM) and atomic-resolution scanning transmission electron microscopy (STEM) were used to directly visualize the microstructure of the h-MXenes. The expansion of interlayer spacing between the $\mathrm{Ti}_3\mathrm{C}_2$ sheets with the introduction of amines can be clearly observed in STEM images (Fig. 3d and Extended Data Fig. 6a,b). Electron energy-loss spectroscopy (STEM-EELS, Extended Data Fig. 6e) reveals the expected distribution of titanium, carbon and nitrogen atoms along the c axis of h-MXenes, and SEM-EDS mapping confirms uniform distribution of terminating groups in macroscopic MXene stacks (Fig. 3e). To visualize organic termination groups, we imaged $\mathrm{Ti}_3\mathrm{C}_2$ (tma) containing heavy sulfur atoms using atomic-resolution annular bright field (ABF) STEM. A double-layered arrangement of tentatively 2-thiophenemethylimido groups was observed between the $\mathrm{Ti}_3\mathrm{C}_2$ sheets (Extended Data Fig. 7f), supporting the ordering of organic groups in h-MXenes.

The lattice constants c estimated from TEM images are systematically smaller than the values of c extracted from XRD data, which can

be explained by the combination of elastic strain in bended h-MXene stacks (Supplementary Fig. 19) and electron beam damage of the organic part during STEM imaging. The imaging of h-MXenes using low-dose cryo-TEM to reduce beam damage, and STEM imaging of non-strained h-MXene slabs prepared by focused ion beam (FIB) milling bring the TEM-derived lattice constants c of h-MXenes in a good agreement with XRD data (Extended Data Fig. 7a–e).

Among various possible h-MXenes, those prepared from diamines, such as ethylenediamine (en) or *N*-methylethylenediamine (nmeda), are of particular interest as two nitrogen atoms can adopt different bonding motifs on the titanium surface. Since the observed interlayer distance in $T_3C_2(en)$ is larger than the length of an extended en molecule, it appears the diamine ligands cannot bridge neighbouring Ti_3C_2 sheets. When diamine h-MXene Ti_3C_2 (nmeda) was treated with dilute hydrobromic acid, XPS showed the formation of $-NRH_3^+$ species (Extended Data Fig. 8a,b). Meanwhile, the (0 0 0 2) peak in the XRD pattern shifted to smaller 2θ angles, indicative of expansion of the interlayer distance after the protonation (Extended Data Fig. 8c). Accordingly, we conclude that in diamine h-MXenes, one nitrogen atom is bonded to the surface of the Ti_3C_2 sheet while the other remains chemically accessible for protonation (Supplementary Discussion 4).

Fano resonances in h-MXenes

Infrared absorption spectroscopy has been routinely used to study vibrations of molecules in SAMs bound to extended metal surfaces²⁴ or metal nanoparticles^{25,26}. Qualitatively, the vibrational spectra of surface-bound alkyl chains resemble spectra of corresponding free molecules because molecular vibrations, for example, C-H stretches in long alkyl groups, are practically not affected by the metal surface. A qualitatively different behaviour is observed for the infrared spectra of h-MXenes: the vibronic absorption bands of *n*-alkylamine exhibit asymmetric line shapes characteristic of Fano resonances^{27,28} (Fig. 4a, Supplementary Discussion 5 and Supplementary Fig. 20). Such resonances emerge when quantum states with discrete spectra, such as vibrational normal modes, coherently couple with a continuum band of states, for example, a plasmon or polariton mode²⁸. The constructive or destructive interference of two paths (Fig. 4b) creates a characteristic asymmetric Fano line shape. In traditional SAMs on flat metal surfaces, or alkyl chains tethered to the surface of individual metal nanocrystals, the coupling of discrete and continuum states is too weak to develop the

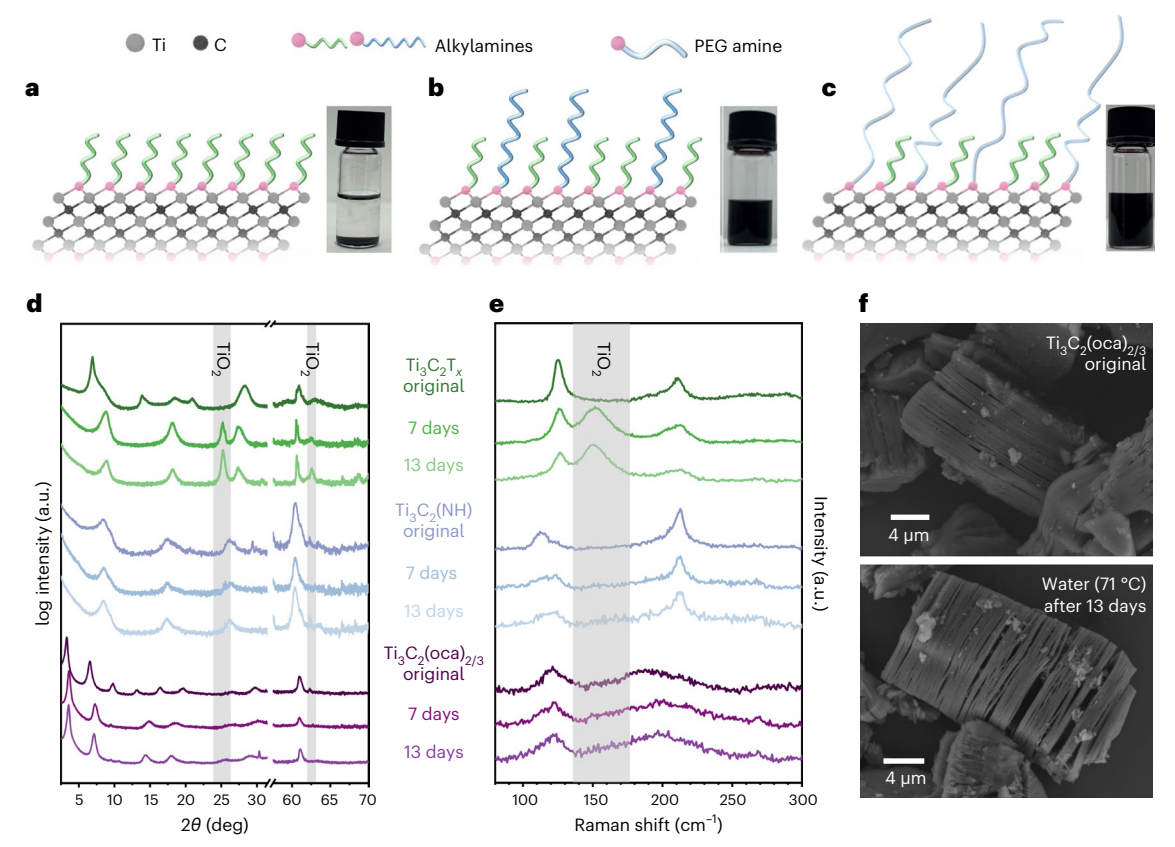


Fig. 5 | Delamination, colloidal dispersion and hydrolytic stability of h-MXenes. a-c, Schematics of delaminated h-MXenes with different types of surface ligands: d-Ti $_3$ C $_2$ (oca) $_{2/3}$ (a), d-Ti $_3$ C $_2$ (oca/ola) $_{2/3}$ (b) and d-Ti $_3$ C $_2$ (ora/PEG $_{1k}$) $_{2/3}$ (c). Insets: photographs of d-Ti $_3$ C $_2$ (oca) $_{2/3}$ in CHCl $_3$ (d) and d-Ti $_3$ C $_2$ (ora/PEG $_{1k}$) $_{2/3}$ in water (c). d,e, Powder X-ray diffraction patterns (d)

and Raman spectra (measured using 785 nm laser excitation) (**e**) of $Ti_3C_2T_x$ (T=0, OH, F), $Ti_3C_2(NH)$ and $Ti_3C_2(oca)_{2/3}$ after exposure to 71 °C pure water for 7 and 13 days. **f**, SEM images of original $Ti_3C_2(oca)_{2/3}$ and after exposure to 71 °C pure water for 13 days.

Fano effect. For h-MXenes, however, the coherent coupling of organic and inorganic components does appear to be sufficiently strong, and we suggest it may originate from plasmonic enhancement of electromagnetic field between the ${\rm Ti_3C_2}$ sheets²⁹. For example, Fano resonances have been reported for molecular vibrations resonantly coupled to plasmonic hotspots with strong optical field enhancement³⁰. From a practical view, the coupling of organic and inorganic components of h-MXenes can be used to facilitate charge, heat and energy transfer across the organic–inorganic interfaces.

Delamination and colloidal dispersion of h-MXenes

h-MXenes with an appropriate choice of surface-bound alkyl chains can be delaminated and dispersed in non-polar solvents to form colloidal solutions (Fig. 5 and Extended Data Fig. 9). Colloidal stabilization in non-polar solvents typically requires a negative free energy of chainsolvent mixing³¹, which causes the hydrocarbon chains to repel one another, thus stabilizing colloidal dispersions³¹. This approach works very well for small nanocrystals where surface curvature allows solvent molecules to efficiently penetrate between surface-bound alkyl chains. At the same time, chain-solvent mixing is known to be inefficient at flat surfaces with densely packed alkyl chains³¹. Accordingly, h-MXenes with only one type of alkyl chain did not show good colloidal stability in non-polar solvents (Fig. 5a). However, simultaneous incorporation of short (for example, octyl) and long (for example, oleyl) chains greatly improved the colloidal stability of h-MXenes by providing room for the free rotation of long chains and efficient interaction with solvent molecules (Fig. 5b). Such combinations of organic ligands, known to the nanocrystal community as 'entropic ligands' 22, can efficiently produce colloidal dispersions of h-MXenes in CHCl₃ with high solid concentrations (Fig. 5b and Extended Data Fig. 9d,e). Raman spectroscopy showed that colloidal h-MXenes possess the same surface groups as their bulk counterparts (Extended Data Fig. 9h). Surface exchange of $Ti_3C_2Br_2$ with the mixture of propylamine and PEG_{1k} amine resulted in Ti_3C_2 MXenes with PEGylated surfaces that are easily dispersed in water (Fig. 5c and Extended Data Fig. 9h).

Improved stability against hydrolysis

MXenes bring many exciting opportunities, but their relatively poor stability against hydrolysis has been a source of legitimate concern and an obvious area for improvement. Different strategies have been explored to stabilize MXenes³³⁻³⁷, but the effect of surface groups on the hydrolytic stability does not yet appear to have been investigated. We performed a comparative study of the hydrolysis rates for traditional $Ti_3C_2T_x$ (T = F, OH, O) MXenes, and for Ti_3C_2 (NH), Ti_3C_2 (pra)_{2/3} and Ti₃C₂(oca)_{2/3} h-MXenes. To minimize the effect of sample preparation conditions, we compared stability of multilayer MXenes of similar size in pure water at room temperature and at 71 °C (Supplementary Fig. 21). A combination of X-ray diffraction, XPS and Raman spectroscopy was used to monitor sample evolution; a full description of our stability study is provided in Supplementary Discussion 6 (Supplementary Figs. 22–30). At room temperature, $Ti_3C_2T_x$, $Ti_3C_2(NH)$ and h-MXenes showed no obvious degradation after 35 days in air-saturated deionized water (Supplementary Fig. 22). However, in accelerated tests at 71 °C, the Ti₃C₂T_x sample showed anatase TiO₂ phase formed due to hydrolysis after 7 days, while no TiO₂ phase was detected in powder X-ray diffraction patterns and in Raman spectra for Ti₃C₂(NH) and

h-MXene samples (Fig. 5d,e and Supplementary Figs. 23 and 24). h-MXenes also showed improved stability in 0.01 M KOH solutions (Supplementary Fig. 25). The alkyl chains provide additional protection against hydrolysis by creating thin hydrophobic barriers, but since we observed a similar stability improvement for Ti₃C₂(NH), Ti₃C₂(pra)_{2/3} and $Ti_3C_2(oca)_{2/3}$, it is reasonable to suggest that surface titanium atoms of amido/imido-terminated MXenes are less susceptible to nucleophilic attack by hydroxyl ions, while hydrophobic surface encapsulation is a complementary and probably secondary effect. As a word of caution, $Ti_3C_2(NH)$ and h-MXenes, as with bulk TiN and TiC (refs. 38,39), are not fully immune to oxidative hydrolysis in hot water. For example, XPS studies show the presence of TiO₂ at the surface of all MXene samples after 1 week of exposure to air-saturated water at 71 °C (Supplementary Fig 27). We attribute this to slow dissolution of titanium species from MXene edges, followed by precipitation of a thin TiO₂ layer. This layer can be only a few nanometres thick because etching the sample surface with Ar₅₀₀⁺ clusters (Ar gas clusters of 500 atoms) efficiently restores the original h-MXene surface (Supplementary Figs. 28-30). Our studies suggest that amido/imido-surface chemistry generally improves MXene resistance against hydrolysis and shows that surface engineering is a viable strategy toward synthesis of functional MXenes with enhanced stability. In parallel with improved stability against hydrolysis, it should be noted that this strategy may not be compatible with some applications of MXenes. For example, bulky organic surface groups can block access to electrocatalytically active surface sites. We should learn from successful examples of organometallic catalysts that efficiently use organic ligands to achieve reaction selectivity without blocking access to the metal site. The nearly endless tailorability of organic components and diverse properties of inorganic MXenes suggest numerous opportunities for future applications, but it will take some time to fully unlock the potential of hybrid organic-inorganic h-MXenes.

Online content

Any methods, additional references, Nature Portfolio reporting summaries, source data, extended data, supplementary information, acknowledgements, peer review information; details of author contributions and competing interests; and statements of data and code availability are available at https://doi.org/10.1038/s41557-023-01288-w.

References

- Anasori, B., Lukatskaya, M. R. & Gogotsi, Y. 2D metal carbides and nitrides (MXenes) for energy storage. *Nat. Rev. Mater.* 2, 1–17 (2017).
- VahidMohammadi, A., Rosen, J. & Gogotsi, Y. The world of two-dimensional carbides and nitrides (MXenes). Science 372, eabf1581 (2021).
- Naguib, M. et al. Two-dimensional nanocrystals produced by exfoliation of Ti₃AlC₂. Adv. Mater. 23, 4248–4253 (2011).
- Ghidiu, M., Lukatskaya, M. R., Zhao, M.-Q., Gogotsi, Y. & Barsoum, M. W. Conductive two-dimensional titanium carbide 'clay' with high volumetric capacitance. *Nature* 516, 78–81 (2014).
- Halim, J. et al. Transparent conductive two-dimensional titanium carbide epitaxial thin films. Chem. Mater. 26, 2374–2381 (2014).
- Kamysbayev, V. et al. Covalent surface modifications and superconductivity of two-dimensional metal carbide MXenes. Science 369, 979–983 (2020).
- Li, Y. et al. A general Lewis acidic etching route for preparing MXenes with enhanced electrochemical performance in non-aqueous electrolyte. *Nat. Mater.* 19, 894–899 (2020).
- 8. Li, M. et al. Element replacement approach by reaction with Lewis acidic molten salts to synthesize nanolaminated MAX phases and MXenes. *J. Am. Chem. Soc.* **141**, 4730–4737 (2019).
- Li, M. et al. Halogenated Ti₃C₂ MXenes with electrochemically active terminals for high-performance zinc ion batteries. ACS Nano 15, 1077–1085 (2021).

- Hope, M. A. et al. NMR reveals the surface functionalisation of Ti₂C₂ MXene. Phys. Chem. Chem. Phys. 18, 5099-5102 (2016).
- Khazaei, M. et al. Novel electronic and magnetic properties of two-dimensional transition metal carbides and nitrides. Adv. Funct. Mater. 23, 2185–2192 (2013).
- Liu, Y., Xiao, H. & Goddard, W. A. Schottky-barrier-free contacts with two-dimensional semiconductors by surface-engineered MXenes. J. Am. Chem. Soc. 138, 15853–15856 (2016).
- 13. Si, C., Zhou, J. & Sun, Z. Half-metallic ferromagnetism and surface functionalization-induced metal-insulator transition in graphene-like two-dimensional Cr₂C crystals. *ACS Appl. Mater. Interfaces* **7**, 17510–17515 (2015).
- Griffith, K. J. et al. Bulk and surface chemistry of the niobium MAX and MXene phases from multinuclear solid-state NMR spectroscopy. J. Am. Chem. Soc. 142, 18924–18935 (2020).
- Harris, K. J., Bugnet, M., Naguib, M., Barsoum, M. W. & Goward, G. R. Direct measurement of surface termination groups and their connectivity in the 2D MXene V₂CT_x using NMR spectroscopy. J. Phys. Chem. C 119, 13713–13720 (2015).
- Kobayashi, T. et al. Nature of terminating hydroxyl groups and intercalating water in Ti₃C₂T_x MXenes: a study by ¹H solid-state NMR and DFT calculations. J. Phys. Chem. C 124, 13649–13655 (2020).
- Beaumier, E. P., Billow, B. S., Singh, A. K., Biros, S. M. & Odom, A. L. A complex with nitrogen single, double, and triple bonds to the same chromium atom: synthesis, structure, and reactivity. *Chem.* Sci. 7, 2532–2536 (2016).
- Paluch, P., Pawlak, T., Amoureux, J.-P. & Potrzebowski, M. J. Simple and accurate determination of X-H distances under ultra-fast MAS NMR. J. Magn. Reson. 233, 56–63 (2013).
- Hillhouse, G. L. & Bercaw, J. E. Reactions of water and ammonia with bis(pentamethylcyclopentadienyl) complexes of zirconium and hafnium. J. Am. Chem. Soc. 106, 5472–5478 (1984).
- Green, M. L. H. A new approach to the formal classification of covalent compounds of the elements. J. Organomet. Chem. 500, 127–148 (1995).
- Anderson, N. C., Hendricks, M. P., Choi, J. J. & Owen, J. S. Ligand exchange and the stoichiometry of metal chalcogenide nanocrystals: spectroscopic observation of facile metal-carboxylate displacement and binding. *J. Am. Chem. Soc.* 135, 18536–18548 (2013).
- Ghidiu, M. & Barsoum, M. W. The {110} reflection in X-ray diffraction of MXene films: misinterpretation and measurement via non-standard orientation. J. Am. Ceram. Soc. 100, 5395–5399 (2017).
- 23. Bain, C. D. et al. Formation of monolayer films by the spontaneous assembly of organic thiols from solution onto gold. *J. Am. Chem.* Soc. **111**, 321–335 (1989).
- Dubois, L. H. & Nuzzo, R. G. Synthesis, structure, and properties of model organic surfaces. *Annu. Rev. Phys. Chem.* 43, 437–463 (1992).
- Badia, A., Cuccia, L., Demers, L., Morin, F. & Lennox, R.
 B. Structure and dynamics in alkanethiolate monolayers self-assembled on gold nanoparticles: a DSC, FT-IR, and deuterium NMR study. J. Am. Chem. Soc. 119, 2682–2692 (1997).
- Hostetler, M. J., Stokes, J. J. & Murray, R. W. Infrared spectroscopy of three-dimensional self-assembled monolayers: N-alkanethiolate monolayers on gold cluster compounds. Langmuir 12, 3604–3612 (1996).
- Luk'yanchuk, B. et al. The Fano resonance in plasmonic nanostructures and metamaterials. *Nat. Mater.* 9, 707–715 (2010).
- Miroshnichenko, A. E., Flach, S. & Kivshar, Y. S. Fano resonances in nanoscale structures. Rev. Mod. Phys. 82, 2257 (2010).
- El-Demellawi, J. K., Lopatin, S., Yin, J., Mohammed, O. F. & Alshareef, H. N. Tunable multipolar surface plasmons in 2D Ti₃C₂T_x MXene flakes. ACS Nano 12, 8485–8493 (2018).

- Agrawal, A. et al. Resonant coupling between molecular vibrations and localized surface plasmon resonance of faceted metal oxide nanocrystals. *Nano Lett.* 17, 2611–2620 (2017).
- 31. Israelachvili, J. N. *Intermolecular and Surface Forces* (Academic Press, 2011).
- 32. Pang, Z., Zhang, J., Cao, W., Kong, X. & Peng, X. Partitioning surface ligands on nanocrystals for maximal solubility. *Nat. Commun.* **10**, 2454 (2019).
- Zhang, J. et al. Freezing titanium carbide aqueous dispersions for ultra-long-term storage. ACS Appl. Mater. Interfaces 12, 34032–34040 (2020).
- Zhang, C. J. et al. Oxidation stability of colloidal two-dimensional titanium carbides (MXenes). Chem. Mater. 29, 4848–4856 (2017).
- Natu, V. et al. Edge capping of 2D-MXene sheets with polyanionic salts to mitigate oxidation in aqueous colloidal suspensions.
 Angew. Chem. 131, 12785–12790 (2019).
- 36. Mathis, T. S. et al. Modified MAX phase synthesis for environmentally stable and highly conductive Ti₃C₂ MXene. ACS Nano **15**, 6420–6429 (2021).
- 37. Wang, X., Wang, Z. & Qiu, J. Stabilizing MXene by hydration chemistry in aqueous solution. *Angew. Chem. Int. Ed.* **60**, 26587–26591 (2021).

- Avgustinik, A. I., Drozdetskaya, G. V. & Ordan'yan, S. S. Reaction of titanium carbide with water. *Powder Metall. Met. Ceram.* 6, 470–473 (1967).
- 39. Vasilos, T. & Kingery, W. Note of properties of aqueous suspensions of TiC and TiN. *J. Phys. Chem.* **58**, 486–488 (1954).
- 40. Limonov, M. F., Rybin, M. V., Poddubny, A. N. & Kivshar, Y. S. Fano resonances in photonics. *Nat. Photonics* **11**, 543–554 (2017).

Publisher's note Springer Nature remains neutral with regard to jurisdictional claims in published maps and institutional affiliations.

Springer Nature or its licensor (e.g. a society or other partner) holds exclusive rights to this article under a publishing agreement with the author(s) or other rightsholder(s); author self-archiving of the accepted manuscript version of this article is solely governed by the terms of such publishing agreement and applicable law.

@ The Author(s), under exclusive licence to Springer Nature Limited 2023

Methods

Synthesis of h-MXenes

Ti₃AlC₃ MAX phases and Cl- and Br-terminated MXenes were synthesized following a modification of a previously reported approach⁶. In brief, Ti₂AlC₂ MAX phase was synthesized by mixing titanium (3.661 g), carbon (0.582 g) and aluminium (0.757 g) (3:1.9:1 molar ratio) powders and pressing this into a pellet. The resulting pellet was heated in an alumina crucible at 1650 °C for 6 hunder a flow of argon. Ti₂AlC₂ (0.5 g) MAX phase was mixed with CdCl₂ or CdBr₂ salts in 1:8 molar ratio using a mortar and pestle. The resulting mixture was heated in an alumina crucible under argon at 610 °C for at least 6 h. The Cl-functionalized MXenes were recovered from the reaction mixture by dissolving excess CdCl₂ and cadmium metal in concentrated aqueous HCl (12.1 M) followed by washing of the solid with deionized water until the washings had neutral pH. The Br-functionalized MXenes were recovered from the reaction mixture by dissolving excess CdBr₂ and cadmium metal in concentrated aqueous HBr for at least 24 h, followed by washing of the solid with deionized water until the washings had neutral pH. The resulting MXene powders were dried under vacuum at 45 °C for >12 h before further use.

Substitution reactions were all performed in a nitrogen-filled glovebox with oxygen and moisture levels below 0.1 ppm unless stated otherwise. The Cl- and Br-terminated MXenes act similarly during the substitution reactions. In a typical reaction procedure, Ti₃C₂Br₂MXene (40 mg) was stirred in a mixture of amine and NaH (24 mg) or 200 μl 2.5 M n-BuLi or 84 mg LiN(Si(CH₃)₃)₂ at 120 °C for 2 days in a pressurized glass vessel. Safety precaution: NaH, n-BuLi and LiN(Si(CH₃)₃)₂ require special care because they can vigorously react with water. Heavy-walled glassware of an appropriate thickness should be used, since the amine may be above its boiling point, for example, propylamine (pra, b.p. 47.8 °C), and H₂ gas is evolved. Alternatively, amine can be deprotonated by NaNH₂ at 120 °C for 1 day using a nitrogen Schlenk line. h-MXenes can be obtained by the addition of Ti₃C₂Br₂ and reaction at 120 °C for another 2 days under nitrogen. As-prepared h-MXenes were washed with toluene and methanol to remove excessive amine, amide and alkali halide by-product. Powder X-ray diffraction patterns and XRF spectra indicate that amines without deprotonating agents do not react with Ti₃C₂Br₂, and NaH itself also does not react with Ti₃C₂Br₂ in heptane at 120 °C (Extended Data Fig. 1b).

Delamination of h-MXenes

A mixture of two amines (for example, pra/ola, pra/PEG_{1k}, oca/ola, with the molar ratio at 9:1 for the short and long chains, respectively) can be deprotonated by n-BuLi and then reacted with bulk Ti₂C₂Br₂ at 120 °C for 2 days to prepare delaminated h-MXenes (Extended Data Fig. 10). Oleyl chains are particularly good at disrupting packing of saturated alkyl chains and stabilizing colloidal dispersions. The as-obtained h-MXenes were washed with anhydrous toluene and methanol then stirred in CHCl₃ or NMF at 70 °C overnight for redispersion. Alternatively, Ti₃C₂Cl₂ was first delaminated following a modification of a previously reported method⁶. In brief, 500 mg Ti₃C₂Cl₂ was immersed in 5 ml of 2.5 M *n*-BuLi solution in a sealed vial. Then, the mixture was stirred at room temperature for 24 h followed by washing with hexane and THF inside a nitrogen-filled glovebox. Then, 100 mg of intercalated powder and 10 ml anhydrous NMF were added in a centrifuge tube, which was sealed while still inside the nitrogen-filled glovebox. After bath sonication (<10 °C to avoid possible oxidation) for 1 h, the supernatant was collected after centrifuging at 352g for 20 min. Finally, the supernatant was centrifuged at 12,600g for 15 min to precipitate the MXenes, leaving small impurities in solution. The surfaces of as-obtained delaminated Ti₃C₂Cl₂ were then modified following the above method for the synthesis of organic-inorganic hybrid MXenes. The obtained product can easily redisperse in chloroform to form a stable colloid. The as-obtained h-MXenes were washed with anhydrous toluene and methanol, and then stirred in a mixture of CHCl₃ and oleylamine at 70 °C overnight for redispersion.

Material characterization

Powder X-ray diffraction patterns were obtained using a MiniFlex benchtop X-ray diffractometer (Rigaku Americas) with a Cu Kα X-ray source (1.5418 Å) operating at 40 kV and 15 mA. XRF analysis was performed with a benchtop energy dispersive Rigaku NEX DE VS X-ray $fluorimeter\ equipped\ with\ a\ Peltier\ -cooled\ FAST\ silicon\ drift\ detector.$ SEM imaging and EDX elemental mapping were performed in a Carl Zeiss Merlin field-emission scanning electron microscope equipped with Oxford Ultim Max 100 silicon drift detectors. Atomic force microscopy (AFM) images were acquired using a Bruker Multimode 8 instrument equipped with a Nanoscope 5 controller. STEM imaging was performed in an aberration-corrected JEOL ARM200CF at the University of Illinois at Chicago, equipped with a cold field emission gun operated at 200 kV, a Gatan Continuum electron energy-loss spectrometer and an Oxford XMAX100TLE X-ray detector, providing a sub-ångström probe-size and 350 meV energy resolution. Solid-state NMR experiments were performed on a 9.4 T (v_0 (1 H) = 400 MHz) Bruker wide-bore NMR magnet equipped with a Bruker Avance III HD console. Experiments were performed with a Bruker 1.3 mm HX probe in double-resonance mode. Raman spectra were obtained with a Horiba LabRamHR Evolution confocal microscope. XPS analysis was performed on a Kratos Axis Nova spectrometer using a monochromatic Al Kα source. Raman (Supplementary Fig. 1) and XPS (Supplementary Discussion 4) measurements are consistent with the bonding motifs revealed by ssNMR, supporting our description of h-MXenes as a combination of amido and imido groups bonded to Ti₃C₂ sheets. Further details of the characterization methods can be found in the Supplementary Information.

Data availability

The data supporting the findings of this study are provided in the Article and its Supplementary Information and are also available from the corresponding author upon reasonable request. Source data are provided with this paper.

References

41. Wallwork, S. C. Introduction to the Calculation of Structure Factors. (University College Cardiff Press, 1980).

Acknowledgements

We thank J. Anderson, H. You, W. Cho, H. Wu, J. Ondry, J. Xie, N. Jiang and A. Ramaanathan for help and valuable discussions. We are also grateful to A. Nelson for a critical reading and editing of the manuscript. h-MXene synthesis and surface functionalization studies were supported by the National Science Foundation under award number DMR-2004880 and Advanced Materials for Energy-Water Systems (AMEWS) Center, an Energy Frontier Research Center funded by the US Department of Energy (DOE), Office of Science, BES. Spectroscopic studies were supported by the Department of Defense Air Force Office of Scientific Research under grant number FA9550-22-1-0283. Several concepts discussed here have been formulated during the preparation of NSF Center for Chemical Innovation (CCI) Proposal for NSF Center for MXenes Synthesis, Tunability and Reactivity (M-STAR). This work made use of the shared facilities at the University of Chicago Materials Research Science and Engineering Center, supported by National Science Foundation under award number DMR-2011854. Parts of this work were carried out at the Soft Matter Characterization Facility of the University of Chicago. Computational studies by M.L. and D.J. were supported by the Fluid Interface Reactions, Structures, and Transport (FIRST) Center, an Energy Frontier Research Center (EFRC) funded by the US DOE, Office of Science, Office of Basic Energy Sciences. F.L. and R.F.K. at University of Illinois Chicago (UIC) were supported by a grant from the National Science Foundation (NSF-DMR 1831406). Acquisition of the UIC JEOL

ARM200CF was supported by an MRI-R2 grant from the National Science Foundation (DMR-0959470). The Gatan Continuum GIF acquisition at UIC was supported by an MRI grant from the National Science Foundation (DMR-1626065). The work used resources of the Center for Nanoscale Materials, a US DOE Office of Science User Facility operated for the DOE Office of Science by Argonne National Laboratory under contract number DE-AC02-06CH11357. Solid-state NMR spectroscopy (B.A. and A.J.R.) was supported by the US DOE, Office of Science, Basic Energy Sciences, Materials Science and Engineering Division. The Ames National Laboratory is operated for the US DOE by Iowa State University under contract number DE-AC02-07CH11358.

Author contributions

C.Z. and D.W. performed and designed the experiments and analysed data. F.L. and R.F.K. performed high-resolution STEM studies and image analysis. B.A. and A.J.R. performed solid-state NMR studies and analysis. H.H. participated in the early stages of the project. Z.Z. contributed to the X-ray diffraction data analysis and AFM studies. M.L. and D.J. performed computational studies. A.S.F. performed XPS measurements. D.V.T. conceived and designed experiments, analysed data and supervised the project. C.Z. and D.V.T. co-wrote the

manuscript. All authors discussed the results and commented on the manuscript.

Competing interests

A patent application has been filed on this technology.

Additional information

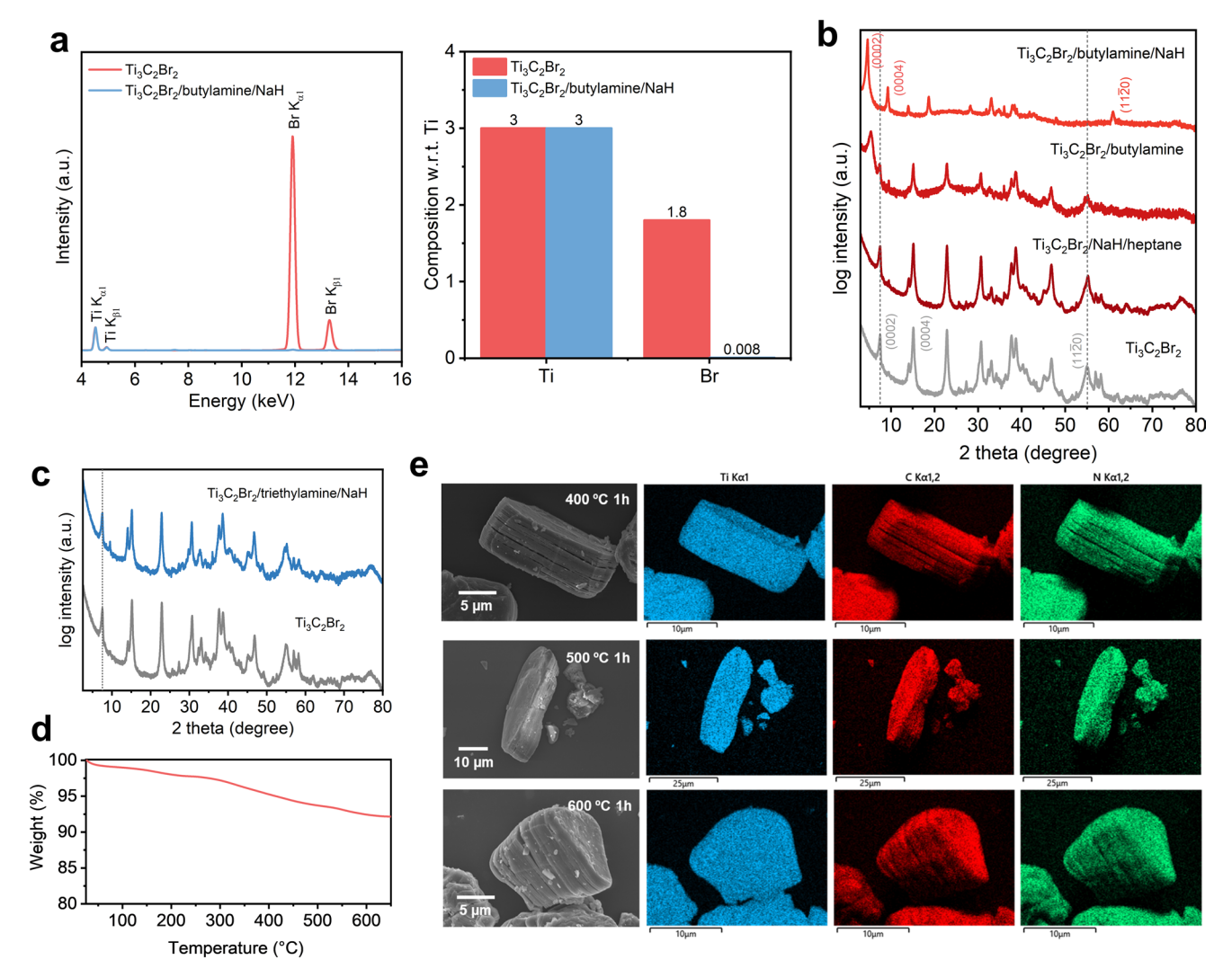
Extended data is available for this paper at https://doi.org/10.1038/s41557-023-01288-w.

Supplementary information The online version contains supplementary material available at https://doi.org/10.1038/s41557-023-01288-w.

Correspondence and requests for materials should be addressed to Dmitri V. Talapin.

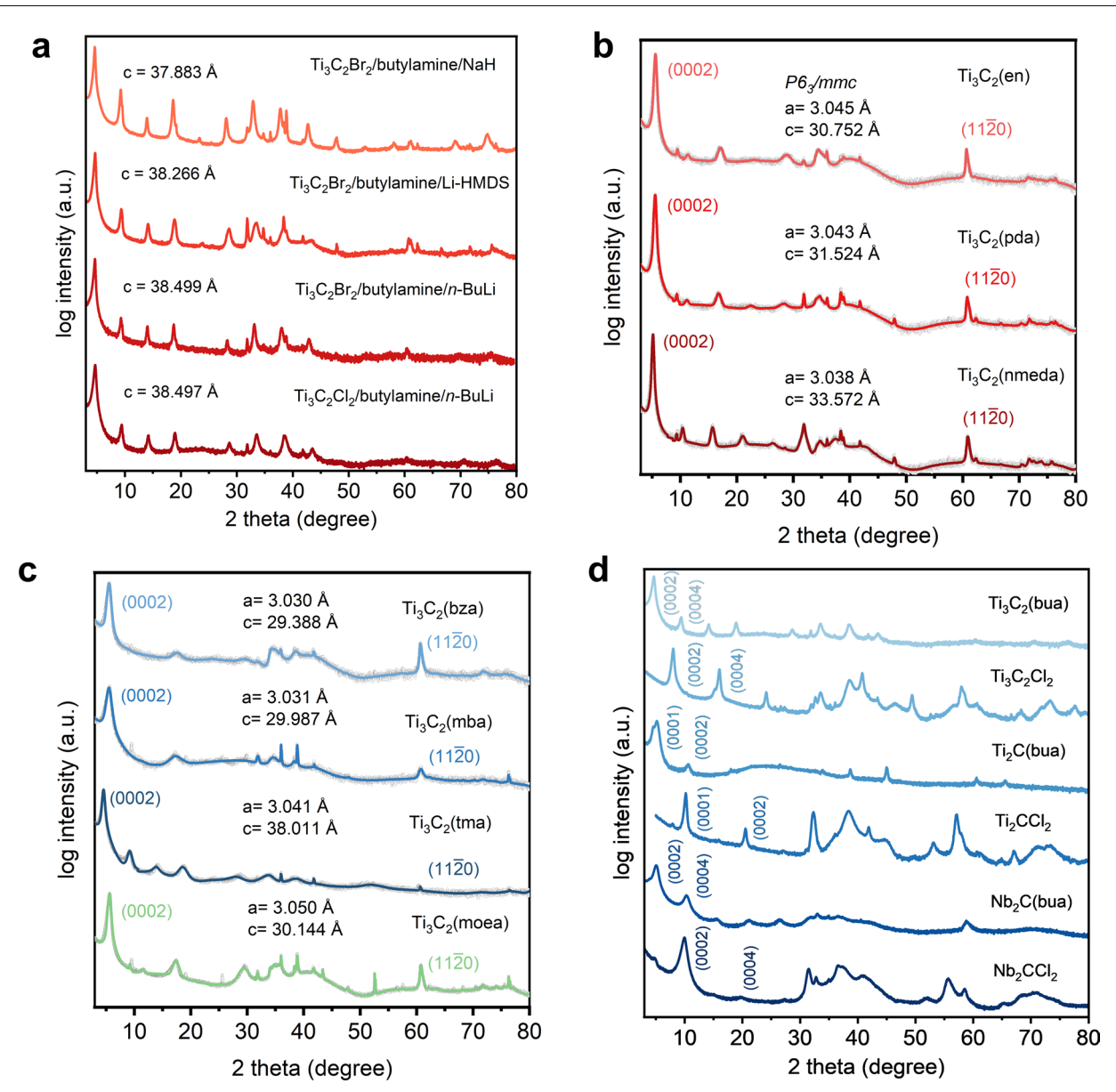
Peer review information *Nature Chemistry* thanks Maria Lukatskaya, Varun Natu and the other, anonymous, reviewer(s) for their contribution to the peer review of this work.

Reprints and permissions information is available at www.nature.com/reprints.



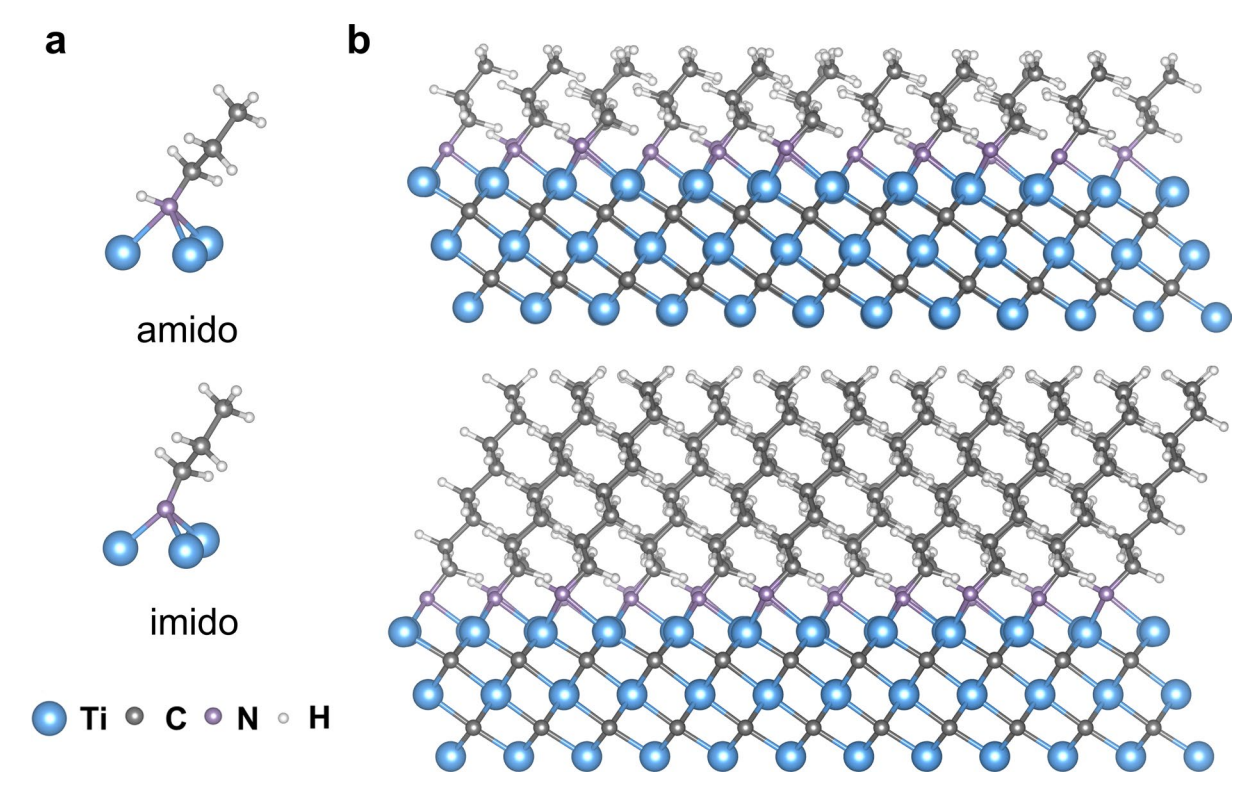
Extended Data Fig. 1 | Surface exchange reaction of Ti $_3$ C $_2$ MXenes with amines and thermal degradation analysis of h-MXenes. a, X-ray fluorescence (XRF) spectral and elemental analysis for the Ti $_3$ C $_2$ Br $_2$ and Ti $_3$ C $_2$ (bua) $_{2/3}$ MXenes. XRF spectra were normalized according to Ti K $_{\alpha 1}$. Based on XRF analysis, Br was completely removed after the surface modification with deprotonated butylamine. b, Powder XRD patterns of products after treatment of Ti $_3$ C $_2$ Br $_2$ with butylamine and NaH at 120 °C for 2 days, as well as the products of control experiments. We observed that Ti $_3$ C $_2$ Br $_2$ barely reacted with NaH in an inert solvent at 120 °C. When treated only with butylamine at 120 °C, Ti $_3$ C $_2$ Br $_2$ is likely to be partially converted or intercalated, as a new peak at 5.4° has emerged, but the majority of Ti $_3$ C $_2$ Br $_2$ is still intact. When butylamine was deprotonated by NaH and then reacted with Ti $_3$ C $_2$ Br $_2$, the (0 0 0 2) peak shifted to 4.65° while the (11 $\overline{2}$ 0) peak

shifted to 60.9° . The absence of diffraction peaks from $Ti_3C_2Br_2$ suggests the reaction was complete, which was confirmed by XRF analysis. \mathbf{c} , Powder XRD patterns of $Ti_3C_2Br_2$ before and after treatment with triethylamine and NaH at $120\,^\circ\mathrm{C}$ for 2 days: The XRD pattern is unchanged, which indicates that no reaction occurred and suggests that deprotonation of amines is crucial to promoting the exchange reaction on MXene surfaces. \mathbf{d} , TGA characterization of $Ti_3C_2(pra)_{2/3}$ MXene. The sample was heated from room temperature (25 °C) to $650\,^\circ\mathrm{C}$ at a rate of $2\,^\circ\mathrm{C}$ min $^{-1}$ under nitrogen. \mathbf{e} , SEM-EDS images of pristine $Ti_3C_2(pra)_{2/3}$ and that after heating up from room temperature (25 °C) to designated temperature at a rate of $20\,^\circ\mathrm{C}$ min $^{-1}$ and hold for 1 hour under nitrogen flow. XRD and Raman characterizations of the annealed h-MXenes are shown in Supplementary Fig. 1.

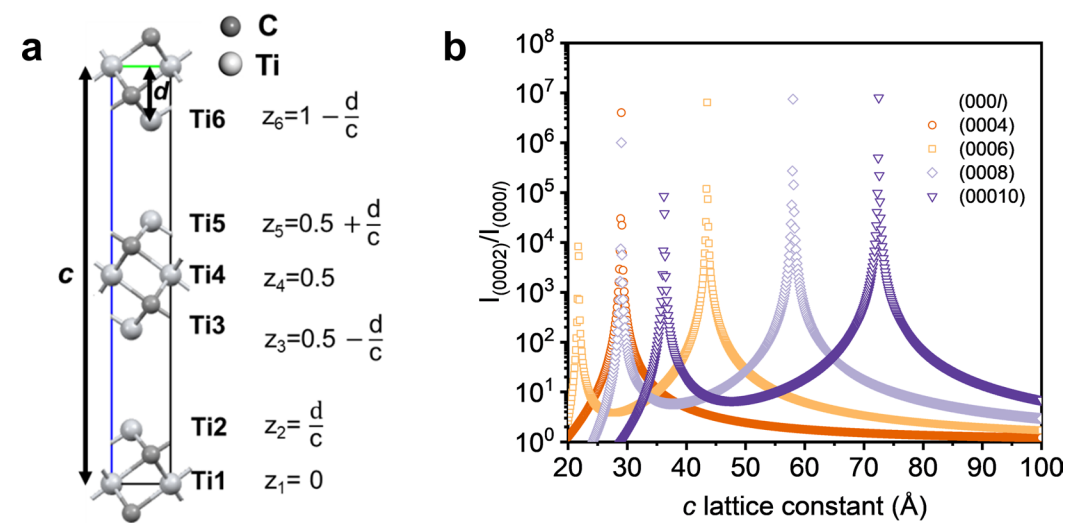


Extended Data Fig. 2 | **Surface exchange reaction of Br- or Cl- terminated MXenes with amines. a**, Powder XRD patterns of $Ti_3C_2(bua)_{2/3}$ prepared by using different halogen terminated MXenes and deprotonating agents. Identical products were obtained using different combinations of starting halogenterminated MXenes and deprotonating agents. **b**, Powder XRD patterns from diamine-modified h-MXenes and their Le Bail fits. **c**, Powder XRD patterns from

aromatic amine- and 2-methoxyethylamine- modified h-MXenes and their Le Bail fits. ${\bf d}$, Powder XRD patterns from different types of Cl-terminated MXenes treated with butylamine and n-BuLi. PXRD patterns suggest that the approach of surface modification can also be applied to other MXenes, *for example*, Ti₂C and Nb₂C MXenes.



 $\textbf{Extended Data Fig. 3} \ | \ \textbf{DFT modeling of h-MX enes. a}, \ \text{Representative snapshots of propyl groups bond to surface Ti atoms in a mido and imido motif, respectively.} \\ \textbf{b}. \ \text{Representative snapshots of propyl or octyl a mido/imido groups bond to surface Ti atoms with tilt angle calculated to be 34° and 35°, respectively.} \\$



Extended Data Fig. 4 | c lattice constant-dependent (0 0 0 l) XRD peak

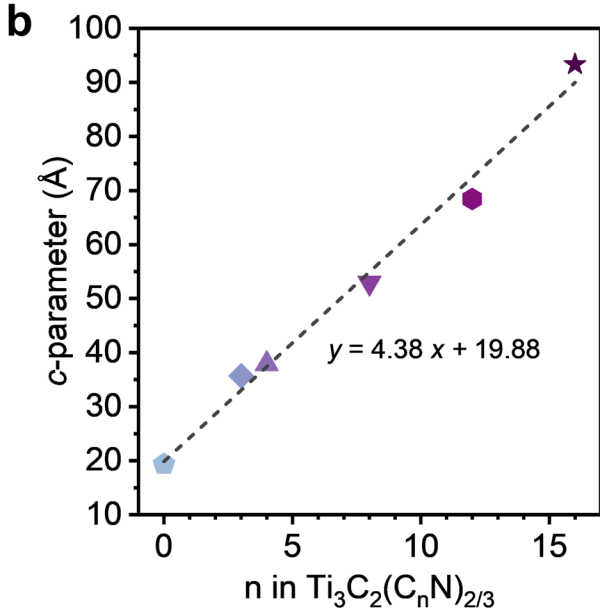
intensity. a, Side view of the unit cells of Ti₃C₂MXene with z coordinates of Ti atoms indicated. **b**, Relationship between the intensity ratio for $(0\ 0\ 0\ 2)/(0\ 0\ 0\ l)$ XRD peaks and the c lattice constant. When the c lattice constant varies, the ratio of the peak intensities for the $(0\ 0\ 0\ 2)$ reflection to those of the $(0\ 0\ 0\ l)$ peaks can change by several orders of magnitude. To quantify these changes, the theoretical peak intensities for each Bragg reflection were calculated using the equation: $l_{nkl} = \left(\sum_{j}^{N} f_{j} \cos\varphi_{j}\right)^{2} + \left(\sum_{j}^{N} f_{j} i sin\varphi_{j}\right)^{2}$, where l is the relative integrated intensity, f is the atomic form factor, and $\varphi_{n} = 2\pi(hx_{n} + ky_{n} + lz_{n})$. Here, the equation was simplified by ignoring light atoms with small atomic numbers Z, including N (Z=7), C (Z=6), and H (Z=1), considering their sufficiently lower $f-Z^{2}$ compared to Ti (Z=22). The imaginary part $\sum_{j}^{N} f_{j} i \sin\varphi_{j}$ is eliminated when a

collection of atoms has a center of symmetry⁴¹. For (0 0 0 *l*) lamella peaks, $\varphi_n = 2l\pi * z_n$. As a result, this equation can be further simplified to

 $I_{hkl} = \left(\sum_{j}^{N} f_{j} \cos(2ln*z_{n})\right)^{2}$. The value of d was found from STEM images to be around 2.4 Å. The correlations between the calculated $(0\,0\,0\,2)/(0\,0\,0\,l)$ peak intensity ratio and the c-lattice constant are shown in Extended Data Fig. 3b. This qualitative analysis helps to understand the non-monotonic variation of peak intensity ratios with c lattice constants among h-MXenes. For example, it explains why the difference between the intensities of $(0\,0\,0\,2)$ and $(0\,0\,0\,4)$ peaks gradually decreases when the c lattice constant increases for alkylimidoterminated $T_{i_3}C_2$ MXenes. It also explains why the $(0\,0\,0\,6)$ peak of $T_{i_3}C_2$ (oca)_{2/3} becomes less intense when the c lattice parameter decreases from 52.93 Å to 49.45 Å in Fig. 5d.

a

h-MXenes	Ti/N ratio	Ti/N ratio
	Elemental analysis*	XPS analysis
Ti ₃ C ₂ (NH)	N/A	3/1.16
$Ti_3C_2(pra)$	3/0.63	3/0.54
Ti_3C_2 (bua)	3/0.71	3/0.72
$Ti_3C_2(oca)$	3/0.82	3/0.75
$Ti_3C_2(hda)$	3/0.88	3/0.74
$Ti_3C_2(en)$	3/1.51	3/1.59
$Ti_3C_2(pda)$	3/1.48	3/1.44
Ti_3C_2 (nmeda)	3/1.15	3/1.29



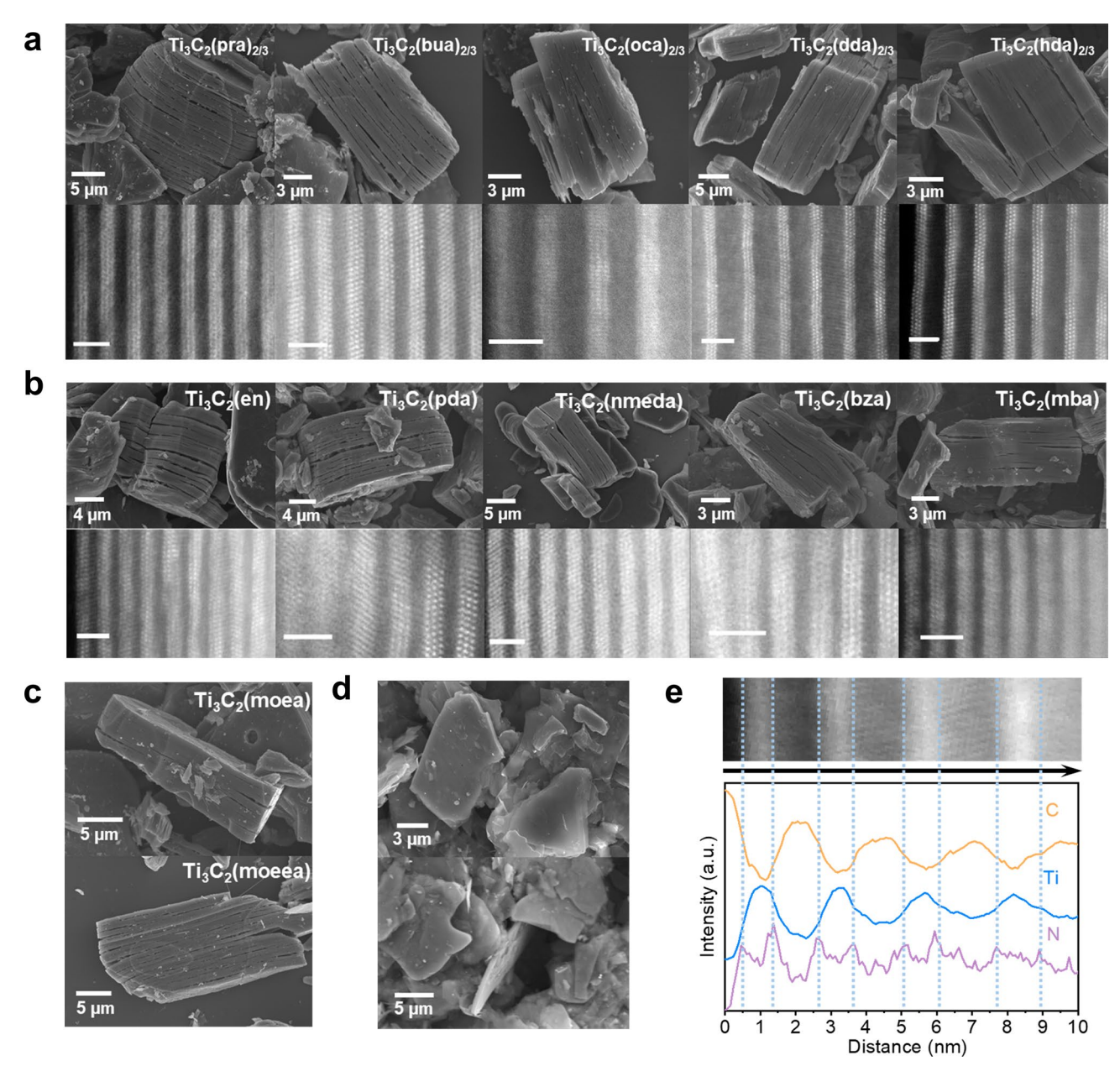
c, Schematic of Ti₃C₂ sheets sandwiched by two layers of alkylimido surface

termination groups. Each crystal unit cell contains two layers of Ti₃C₂ sheets and

 $30 \frac{1}{20} \frac{1}{10} \frac{1}{0} \frac{1}{0}$

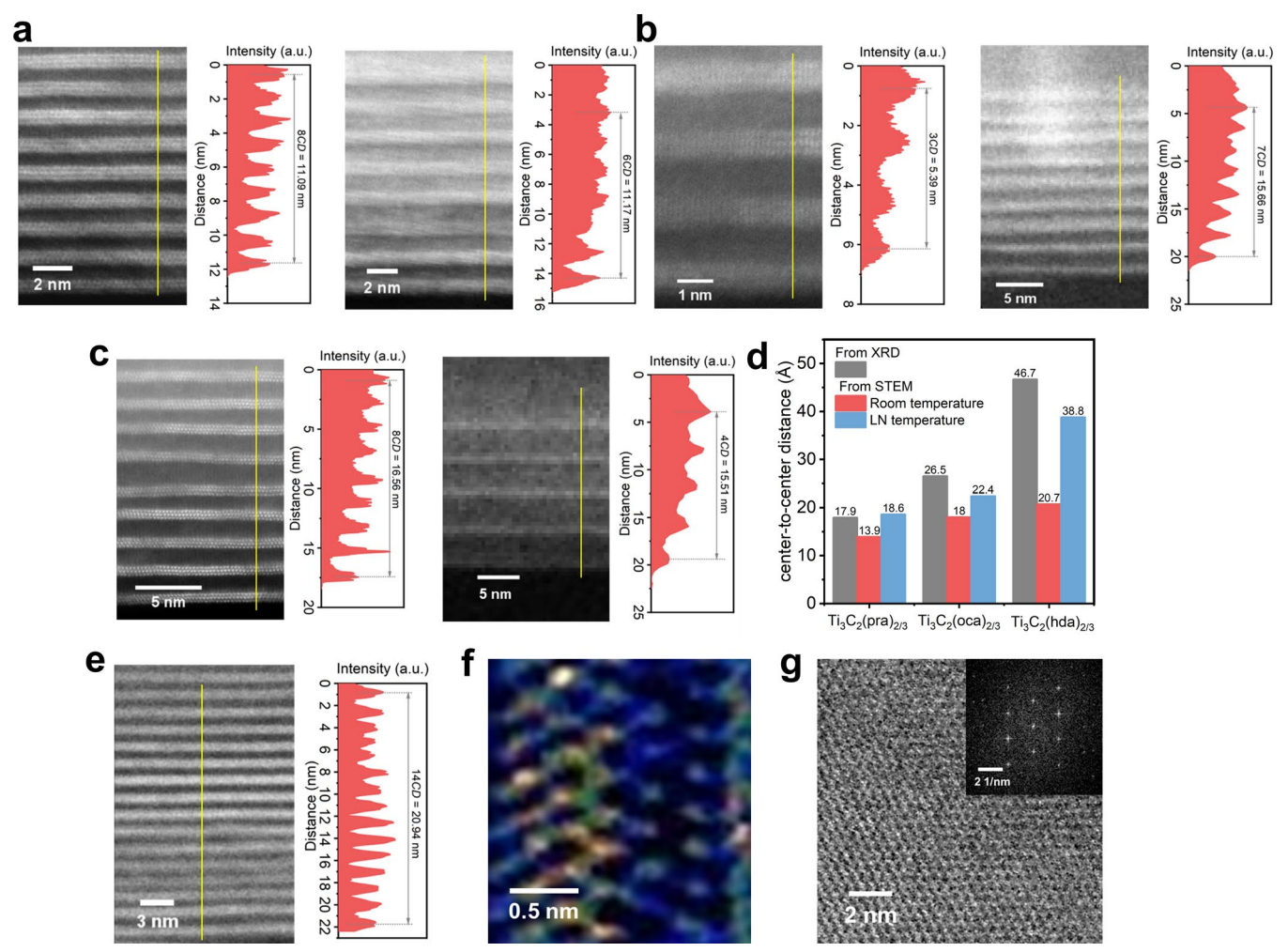
alkyl chain layer thickness 1.10 $\mathring{\mathbf{A}} \times \mathbf{n}$

four layers of surface termination groups. If $Ti_3C_2(NH)$ is used as the reference to account for contributions from Ti-N bonds and the van der Waals gaps, then the slope of Fig. 3b, i,e. 4.38 Å per CH_2 in the alkyl chain, corresponds to four times the thickness of a single alkyl monolayer. Therefore, each CH_2 unit appears to increase the thickness of the alkyl chain layer by -1.10 Å. As the theoretical length of a fully extended alkyl chain with all-*trans* conformations is -1.27 Å per CH_2 group 23 , the tilt angle θ of organic surface group can be calculated to be arccos(1.10 Å/1.27 Å)=30°.



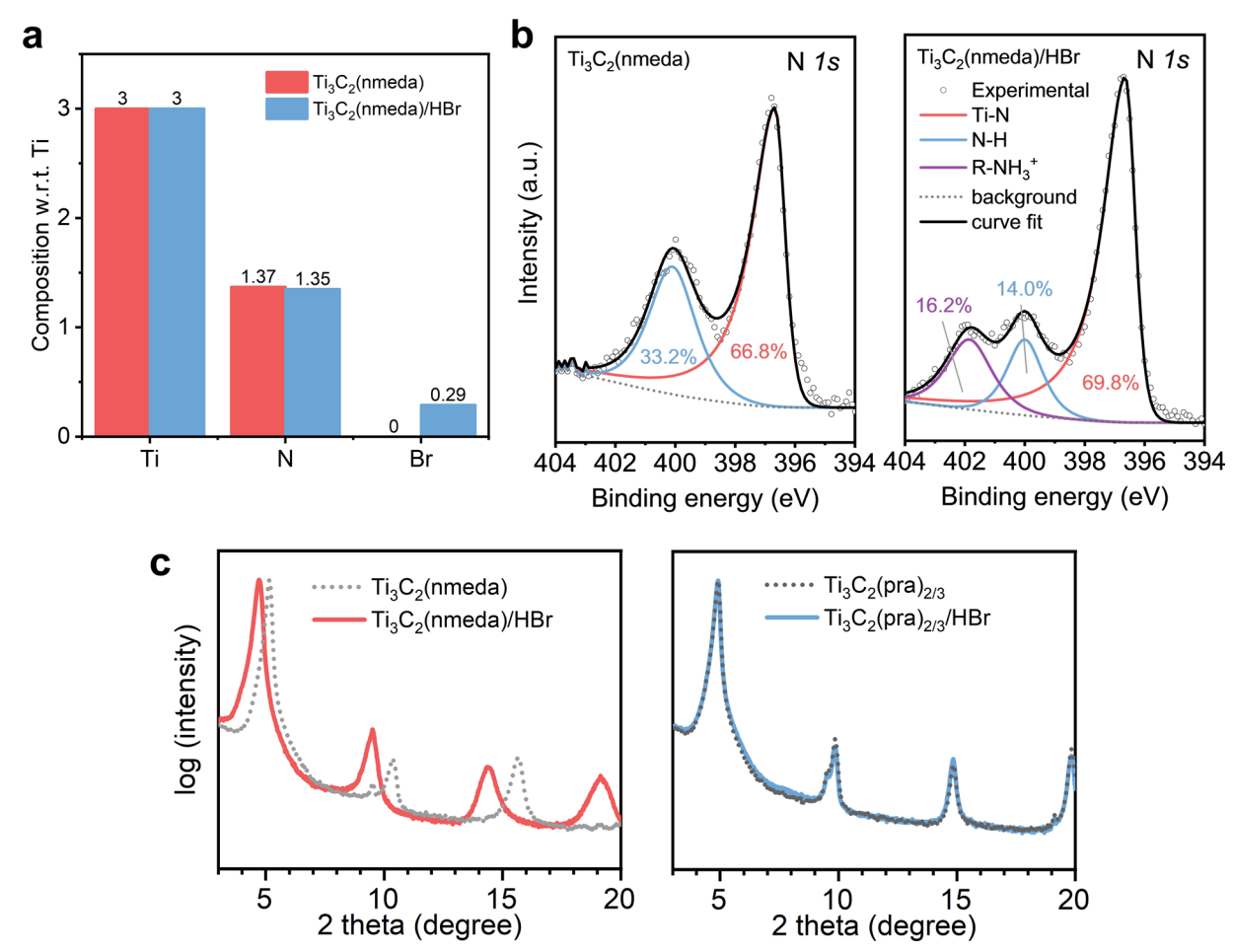
Extended Data Fig. 6 | **SEM and LAADF-STEM images of h-MXenes.** SEM and LAADF-STEM images of **a**, alkylamine-, **b**, diamine- and aromatic-amine-modified h-MXenes (scale bar in STEM images is 2 nm). The systematically smaller d-spacings measured from STEM images in comparison with powder X-ray diffraction patterns is attributed to electron beam-induced damage and strain in bended h-MXene stacks used for imaging, as confirmed by cryo-STEM

imaging of microtomed h-MXene samples which showed much better agreement of interlayer distances with powder XRD data (Extended Data Fig. 5a–c). \mathbf{c} , SEM images of PEG-amine-modified h-MXenes. \mathbf{d} , SEM images of Ti $_3$ C $_2$ (bua) $_{2/3}$ MXenes prepared with n-BuLi as deprotonating agent. \mathbf{e} , STEM-EELS elemental analysis (line scan) of Ti $_3$ C $_2$ (dda) $_{2/3}$ MXene.



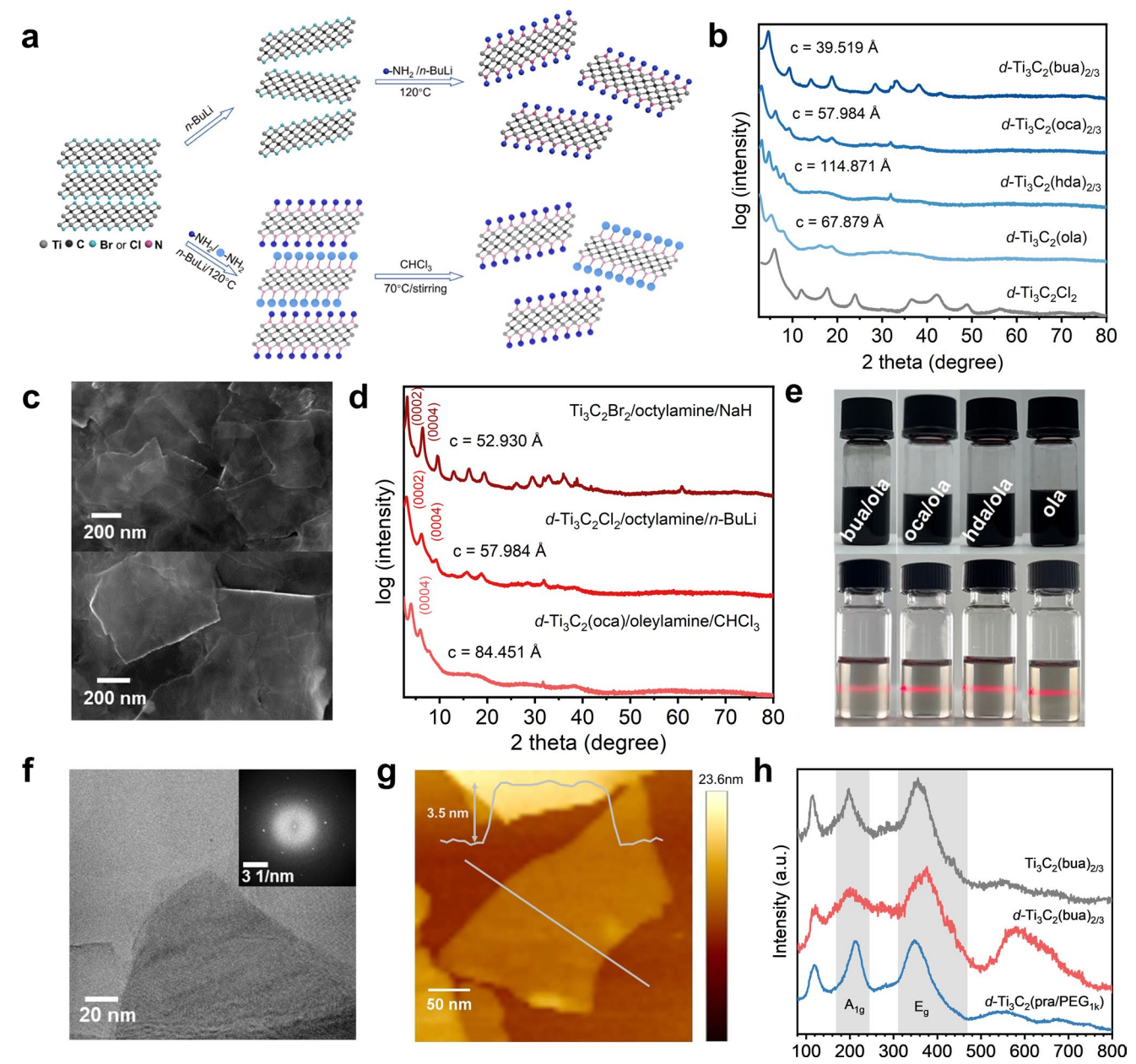
Extended Data Fig. 7 | **STEM images of h-MXenes. a**, LAADF-STEM images of $Ti_3C_2(pra)_{2/3}$ MXene measured at room temperature (left) and at liquid nitrogen temperature (right) with average center-to-center distances (*CD*) of 13.86 Å and 18.61 Å, respectively. (XRD: 17.85 Å) **b**, LAADF-STEM images of $Ti_3C_2(oca)_{2/3}$ MXene measured at room temperature (left) and at liquid nitrogen temperature (right) with average *CD* of 17.97 Å and 22.40 Å, respectively. (XRD: 26.47 Å) **c**, LAADF-STEM images of $Ti_3C_2(hda)_{2/3}$ MXene measured at room temperature (left) and at liquid nitrogen temperature (right) with average *CD* of 20.70 Å and 38.78 Å, respectively. (XRD: 46.67 Å) **d**, Comparison of center-to-center distances obtained from XRD and STEM at room and liquid nitrogen (LN) temperature,

 $\label{eq:continuous} \begin{array}{l} \textbf{e}, \text{LAADF-STEM} \, \text{image} \, \text{of} \, \text{a} \, \text{thin} \, \text{h-MXene} \, \text{slab} \, \text{prepared} \, \text{by} \, \text{focused} \, \text{ion} \, \text{beam} \, \\ \text{(FIB)} \, \text{milling} \, \text{of} \, \text{Ti}_3 \text{C}_2 (\text{pda}) \, \text{MXene} \, \text{measured} \, \text{at} \, \text{room} \, \text{temperature} \, \text{with} \, \text{average} \, \\ \text{CD} \, \text{of} \, \text{14.96 Å} \, (\text{XRD:} 15.76 Å). \, \textbf{f}, \, \text{Inverted} \, \text{ABF-STEM} \, \text{images} \, \text{of} \, \text{Ti}_3 \text{C}_2 (\text{tma}) \, \text{showing} \, \\ \text{double-layered} \, \text{2-thiophenemethylimido} \, \text{group} \, \text{in} \, \text{between} \, \text{Ti}_3 \text{C}_2 \, \text{sheets}. \\ \text{The visualization} \, \text{of} \, \text{S} \, \text{atoms} \, \text{is} \, \text{still} \, \text{challenging} \, \text{because} \, \text{they} \, \text{are} \, \text{relatively} \, \\ \text{light} \, \text{as} \, \text{compared} \, \text{to} \, \text{Ti} \, \text{and} \, \text{less ordered} \, \text{than} \, \text{Ti}_3 \text{C}_2 \, \text{sheets}; \, \text{beam broadening} \, \\ \text{upon entering} \, \text{less ordered} \, \text{material} \, \text{will} \, \text{also} \, \text{reduce} \, \text{our} \, \text{ability} \, \text{to} \, \text{visualize} \, \text{S} \, \\ \text{embedded} \, \text{inside} \, \text{an} \, \text{aromatic ring}. \, \text{The} \, \text{Ti/S} \, \text{ratio} \, \text{was} \, \text{determined} \, \text{to} \, \text{be} \, 3/0.66 \, \text{by} \, \\ \text{XRF} \, \text{analysis.} \, \textbf{g}. \, \, \text{ABF-STEM} \, \text{image} \, \text{of} \, \text{d-Ti}_3 \text{C}_2 (\text{bua})_{2/3} \, \text{viewed} \, \text{along} \, [0001] \, \text{direction}. \\ \text{Fast Fourier transform} \, (\text{FFT, inset)} \, \text{showing} \, \text{hexagonal symmetry} \, \text{of} \, \text{the} \, \text{flake}. \\ \end{aligned}$



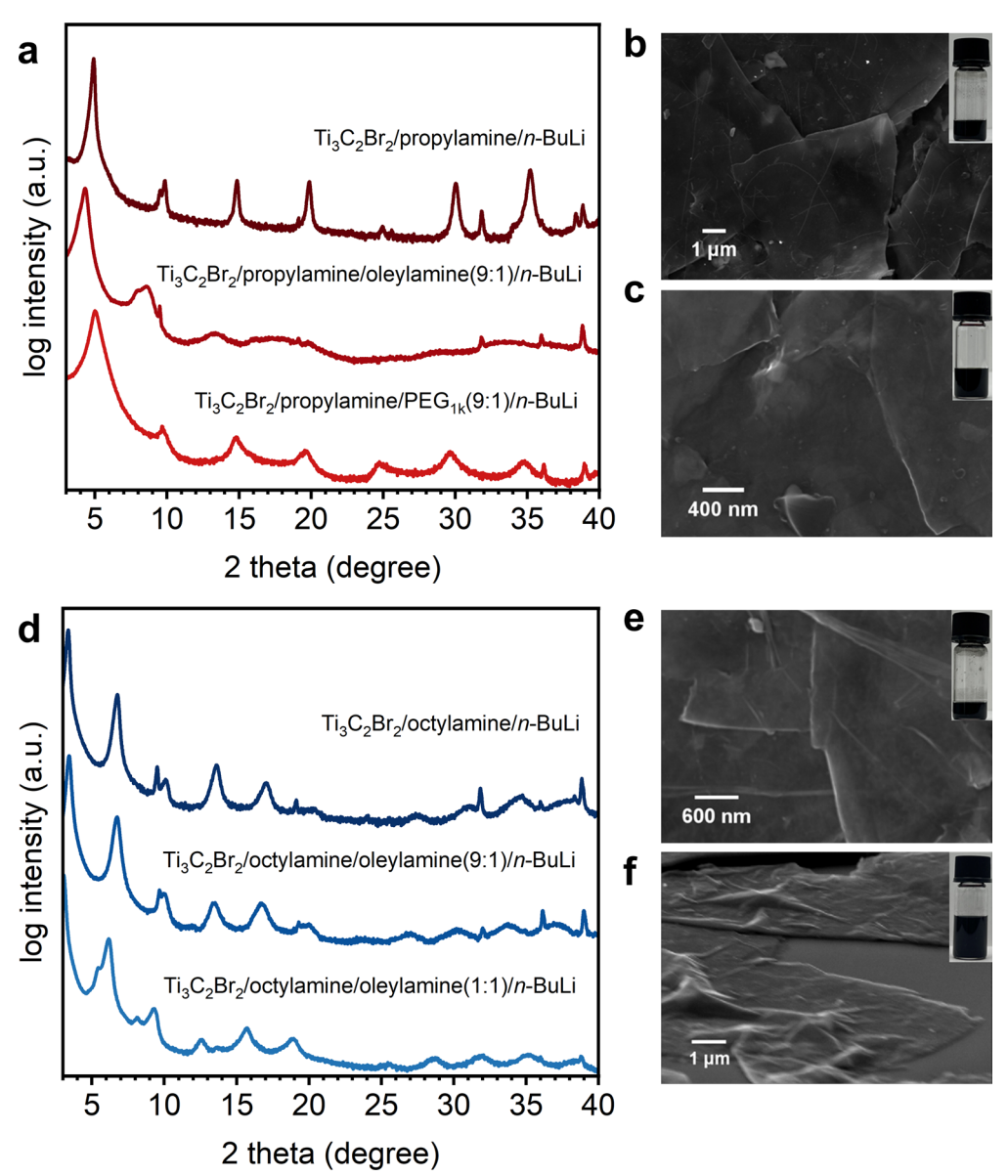
Extended Data Fig. 8 | **Analysis of h-MXenes before and after HBr treatment. a**, XRF and **b**, XPS analysis of Ti_3C_2 (nmeda) h-MXenes before and after HBr treatment. An extra peak at -402 eV appeared after HBr treatment, which was assigned to R-NH₃*. In combination with XRF results and our analysis, we speculate that one nitrogen in diamine h-MXenes is bonded to the Ti_3C_2 surface while the other remains chemically accessible for protonation, or that both nitrogen atoms can be bonded to the same MXene sheet. **c**, Powder XRD patterns of Ti_3C_2 (nmeda) and Ti_3C_2 (pra)_{2/3} before and after HBr treatment. The (0 0 0 2)

peak in the XRD pattern of Ti_3C_2 (nmeda) shifted to smaller 2θ angles, indicating expansion of the interlayer distance after protonation. In comparison, the (0 0 0 2) peak of HBr post-treated Ti_3C_2 (pra) $_{2/3}$ does not shift. The (0 0 0 2) peak of Ti_3C_2 (pra) $_{2/3}$ did not shift to larger 2θ angles after HBr post-treatment, which provides additional evidence that terminating groups are strongly covalently bonded to Ti_3C_2 surface. If the organo-amines were present as intercalated ammonium cations, the HBr treatment would cause replacement of ammonium ions for protons.



Extended Data Fig. 9 | **Delamination of h-MXenes. a**, Schematic process of the preparation of delaminated h-MXenes. **b**, Powder XRD patterns of different delaminated h-MXenes. **c**, SEM images of delaminated $Ti_3C_2(hda)_{2/3}$ h-MXene prepared by reacting delaminated $Ti_3C_2(D_1$ with deprotonated hexadecylamine. **d**, Powder XRD patterns of bulk $Ti_3C_2(oca)_{2/3}$, and d- $Ti_3C_2(oca)_{2/3}$ before and after oleylamine treatment. The films prepared from delaminated h-MXene solutions showed X-ray diffraction patterns with (0 0 0 l) peaks shifted to smaller 2 θ angles as compared to their bulk counterparts, and the ($11\overline{2}0$) peak vanished, as

expected for re-stacked MXenes with randomly rotated individual sheets 22 . \mathbf{e} , Photographs of stable colloidal solutions of delaminated h-MXenes dispersed in CHCl $_3$ at high concentrations (top) and in dilute solutions, showing Tyndall scattering. \mathbf{f} , TEM image of d-Ti $_3$ C $_2$ (oca/ola) $_{2/3}$ MXene flakes deposited from a colloidal solution. (Inset) Fast Fourier transform (FFT) showing the crystallinity and hexagonal symmetry of the individual flake. \mathbf{g} , AFM image of the monolayer d-Ti $_3$ C $_2$ (hda) $_{2/3}$. \mathbf{h} , Raman spectra of Ti $_3$ C $_2$ (bua) $_{2/3}$, d-Ti $_3$ C $_2$ (bua) $_{2/3}$, and d-Ti $_3$ C $_2$ (pra/PEG $_{1k}$) $_{2/3}$.



Extended Data Fig. 10 | **Delamination of bulk Br-terminated MXenes using deprotonated mixed amines.** Mixed amines propylamine/oleylamine or propylamine/PEG_{1k} (9:1) were deprotonated by n-BuLi and then reacted with $Ti_3C_2Br_2$ (bulk powders) at $120\,^{\circ}C$. **a**, powder XRD patterns of h-MXenes with mixed termination groups. SEM image of the h-MXenes with **b**, pra/ola and **c**, pra/PEG_{1k} mixed termination groups and (inset) photograph of the colloidal dispersion in CHCl₃(**b**) or NMF (**c**). **d**, Mixed amines octylamine/oleylamine

 $(9:1 \, or \, 1:1) \, were \, deprotonated \, by \, \textit{n}\text{-BuLi} \, and \, then \, reacted \, with \, Ti_3C_2Br_2 \, (bulk \, powders) \, at \, 120 \, ^{\circ}\text{C}. \, When the \, molar \, ratio \, of \, octylamine/oleylamine is increased \, from \, 9:1 \, to \, 1:1, \, the \, XRD \, patterns \, can \, be \, deconvoluted \, to \, two \, sets \, of \, XRD \, peaks, \, which \, can \, be \, assigned \, to \, separate \, contributions \, from \, d\text{-}Ti_3C_2(oca/ola) \, and \, d\text{-}Ti_3C_2(ola). \, SEM \, image \, of \, the \, hMXenes \, with \, \textbf{e}, \, oca/ola \, (9:1 \, in \, precursor) \, and \, \textbf{f}, \, oca/ola \, (1:1 \, in \, precursor) \, mixed \, termination \, groups \, and \, (inset) \, photograph \, of \, the \, colloidal \, dispersion \, in \, CHCl_3.$